Federal University of Santa Catarina

Technology Centre

Department of Automation and Systems Engineering

Thermal Elastic Model for Ball Screws

Igor Medeiros Benincá

Aachen, July/ 2019

Igor Medeiros Benincá

Thermal Elastic Model for Ball Screws

Final Project Work submitted to the Federal University of Santa Catarina as a requirement for approval in the compulsory discipline ***DAS 5511: Projeto de Fim de Curso*** of the Control and Automation Engineering degree course .

Advisor: Prof. Dr. Marcelo De Lellis Costa de Oliveira

Aachen

2019

Igor Medeiros Benincá

Thermal Elastic Model for Ball Screws

This final project work was judged in the context of the discipline DAS5511: Final Project Work and APPROVED in its final form by the Control and Automation Engineering Course.

Florianópolis, _____

_____

Prof. Dr. Marcelo De Lellis Costa de Oliveira (Advisor)
Automation and Systems Department of the Federal University of Santa Catarina

_____

Florian Kneer, M.Sc. RWTH. (Institute Advisor)
Laboratory for Machine Tools and Production Engineering of the RWTH Aachen University

_____

Gustavo Artur De Andrade (Appraiser)
Automation and Systems Department of the Federal University of Santa Catarina

_____

Gabriel Ratto Goulart (Debater)
Automation and Systems Department of the Federal University of Santa Catarina

_____

Luís Artur Kretzer Tavares Sobral (Debater)
Automation and Systems Department of the Federal University of Santa Catarina

Aachen

2019

DISCLAIMER

The following final project work contains confidential data of Werkzeugmaschinenlabor WZL der RWTH Aachen. Publications and reproductions of the Final Project Work - even in excerpts - are not permitted without the express permission of Werkzeugmaschinenlabor WZL der RWTH Aachen. The final project work is only available to the proofreaders and the members of the examination board.

Now I'm a scientific expert;
that means I know nothing about absolutely everything.

Arthur C. Clarke, 2001: A Space Odyssey

RESUMO

Fusos de esferas recirculantes são mecanismos que convertem movimento rotacional em movimento translacional. Esses consistem de três componentes básicos – fuso, castanha e esferas. Fusos de esferas são amplamente usados em máquinas-ferramenta, robôs e equipamentos de montagem de precisão. A principal vantagem destes componentes é a sua alta precisão de posicionamento, que é influenciada por inúmeros parâmetros, entre os quais a rigidez axial. Em altas velocidades, os efeitos térmicos são condicoes fundamentais relacionadas à precisão de posicionamento e estabilidade dinâmica. O aumento da temperatura e o gradiente térmico entre o parafuso, as esferas e as porcas resultam em variações geométricas e, consequentemente, variações na rigidez axial. Assim, este trabalho apresenta uma estratégia de modelagem numérica para prever a rigidez axial em sistemas de fusos de esferas devido a variações de temperatura utilizando um modelo baseado em análises termo-elásticas por elementos finitos (FEA) para fusos de esferas recirculantes. Para o validamento do modelo, um experimento prático e um sistema de monitoramento foram desenvolvidos a fim de se reproduzir condições reais de operação destes mecanismos e também para a aquisição de valores reais de deslocamento e força.

Palavras-chave: fricção, modelo matemático, fusos de esferas recirculantes

ABSTRACT

Ball screws are mechanisms that convert rotational motion into translational motion. These consist of three basic components - screw, nut and balls in a thread between them. Ball screws are widely used in machine tools, robots and precision assemblies equipment. The main advantage of these components is the high positioning accuracy, that is influenced by numerous parameters, among which is the axial stiffness. At high speeds, thermal effects are fundamental conditions related to positioning accuracy and dynamic stability. The temperature increase and the thermal gradient between the screw, the balls and the nuts result in geometrical variations and, consequently, variations in the axial stiffness. Thus, this work presents a numerical modelling strategy to predict the axial stiffness in ball screws systems due to temperature variations using a thermal-elastic finite element analyses (FEA)-based model for double nut-ball screw drives. For the survey of the model, a practical experiment and a monitoring system were developed in order to reproduce the real operating conditions of these mechanisms and also for the acquisition of real values of displacement and force.

Keywords: Ball screw, Thermal-elastic model, axial stiffness

LIST OF FIGURES

LIST OF TABLES

NOMENCLATURE

Acronyms

Symbol	Description	Units
APDL	ANSYS Parametric Design Language	–
CNC	Computer Numeric Control	–
DAQ	Data Acquisition	–
DOF	Degrees of Freedom	–
FE	Finite Element	–
FEA	Finite Element Analysis	–
FEM	Finite Element Method	–
LabVIEW	Laboratory Virtual Instrument Engineering Workbench	–
LVDT	Linear Variable Differential Transformer	–
NC	Numeric Control	–
NI	National Instruments	–
OPC	Open Platform Communications	–
PLC	Programmable Logic Controller	–
RWTH	Aachen University of Technology (German: *Rheinisch-Westfälische Technische Hochschule Aachen*)	–
TDMS	Technical Data Management Streaming	–
UFSC	Federal University of Santa Catarina (Portuguese: *Universidade Federal de Santa Catarina*)	–

WZL	Laboratory for Machine Tools (German: *Werkzeugmaschinenlabor*)	–

Greek Symbols

Symbol	Description	Units
α	contact angle	–
β	inverse of air temperature	K^{-1}
ΔT_x	difference between the reference temperature and the axial temperature at the position x	K
μ	friction coefficient	–
ω	angular speed	s^{-1}
v_{air}	kinematic air viscosity	m/s^2
φ	lead angle	–

Roman Symbols

Symbol	Description	Units
$[B]$	gradient matrix	–
$[H]$	matrix for convective boundary conditions	W/K
$[K]$	heat stiffness matrix	W/K
$\{R_B\}$	total structure heat flux vector	W
$\{R_H\}$	total structure boundary convection vector	W
$\{R_Q\}$	total structure heat generation vector	W
$\{T\}$	total structure temperature vector	K
A	heat emitting surface	m^2
A_x	cross section area in position x	m^2
c	specific heat capacity	J/Kkg

D_{nut}	nut body outer diameter	mm
d_o	screw diameter	mm
E	elastic coefficient module	N/m^2
E_n	n-element	–
F	sum of forces on the rolling elements	N
F_{ax}	axial load	N
F_n	contact normal load	N
$F_{T,x}$	thermal equivalent force in axial position x	N
G_r	Grashof number	–
H	heat inflow	W
h	convective heat transfer coefficient	W/m^2K
K	stiffness matrix	N/m
k	material thermal conductivity	W/mK
k_{air}	thermal air conductivity	W/mK
M_{rn}	frictional torque of the nut	Nm
N_{comb}	free and forced convection Nusselt number	–
N_{forced}	forced convection Nusselt number	–
N_{free}	free convection Nusselt number	–
N_i, N_j	shape functions	–
N_u	Nusselt number	–
P_r	Prant number	–
Q	heat supply	W
q	heat flux	W/m^2

Q_{ns}	nuts and screw shaft heat generation	W
Q_n	nut heat generation	W
Q_s	screw shaft heat generation	W
R_a	Raylight number	–
r_c	action radius	m
R_e	Reynolds number	–
s_{sur}	surface linear speed	ms^{-1}
T_{inf}	fluid temperature	K
T_{air}	air temperature	K
T_s	surface temperature	K

SUMMARY

1 INTRODUCTION

The global market for industrially manufactured products is a dynamic market in which companies have to compete strategically for market share. A competitive product must have maximum customer benefit and be produced as economically as possible. Shorter product life cycles also provide unexpected production modifications, which leads to a change in the production structures [1].

Machine tools are complex mechanical assemblies made up of a large number of components. These include linear guides of individual machine axes, rotary bearings, drive systems and control components. In addition, modern machine tools are expected to consistently produce the highest quality under stable load in stable processes. On the other hand, machine tools demand a high level of working accuracy and high performance. Working accuracy influences the dimensional accuracy of the manufactured product, which is decisive for the value and quality of the product.

The accuracy of a machine tool depends mostly on the axis control systems being well-adjusted to the mechanical position systems. Ball screw-based linear positioning systems represent one of the key components in high-performance mechanical assemblies and machines, where high speed and axial stiffness are required for a working behavior of a machine tool [2]. According to [3], currently, high speed ball screws can reach 100 m/min of linear speed and accelerations up to 2 g. Friction forces and thermal behavior are crucial in these demanding working conditions.

The problem is, however, that machine tools consist of many machine components, which makes accurate predictions of thermal-elastic behavior very complex. For this reason, all machine components need to be independently examined in order to build a predictive model for the machine as a whole, piece by piece [1].

Ball screws nowadays are widely employed in high-speed and high-precision machine tools, and knowledge of the thermal-elastic behavior of this machine component is indispensable to create a complex prediction model. Since ball screws represent a heat source as an active machine component, understanding its thermal behavior leads to geometrical variations prediction and, consequently to machine accuracy.

1.1 Goals and specifications

In this Final Project Work the goal is to develop a mathematical model for the prediction and simulation of thermal and elastic behavior in ball screws mechanisms. The model must be integrated into the structural software MTPlus created at the Laboratory of Machine Tools and Production Engineering. It was developed to evaluate axial stiffness without considering any thermal behavior. To evaluate the mathematical model, an experiment and a monitoring system are also necessary. This can provide the machine manufactures with several advantages in position accuracy, since thermal compensations are typically a significant phenomenon which position controllers must cope with.

1.2 Correlation with the Control and Automation Engineering Course

As can be seen in Chapter 2, this final project work was made with the research group of Machine Tools in the Laboratory for Machine Tools and Production Engineering of RWTH Aachen, whose purpose is to optimize machine tools and process monitoring strategies as well as to provide process diagnosis using machine data and its influences on the life time of machining components. Essentially, these applications require the development of solutions which integrate software programming, sensors data acquisition, hardware implementation, and, furthermore, data analyzes for optimization.

The group works with topics on manufacturing systems based on which the Control and Automation Engineering undergraduate course at UFSC was created back in the 90's: the multi-disciplinary convergence of electrical, mechanical and computing engineering fields in order to use sensors to measure and develop systems to control, supervise and optimize the processes chain. Nowadays, the Control and Automation Engineering expertise has become indispensable in this digital era through the concept of Industry 4.0.

Therefore, this final project work involves four big Control and Automation Engineering areas: supervisory systems, sensors instrumentation, data acquisition systems, and mathematical modeling programming. These areas cover many disciplines of the Control and Automation undergraduate course at the Federal University of Santa Catarina. The engineering knowledge required to accomplish this final project work was accumulated since the first semester of studies.

2 THE INSTITUTE AND THE RESEARCH INFRASTRUCTURE

In order to provide information about where this final project work was made, this chapter presents the Laboratory for Machine Tools and Production Engineering of RWTH Aachen (from the German, *Werkzeugmaschinenlabor WZL der RWTH Aachen*, Figure 1), the technology research institute which employed the author as Research Assistant.

Figure 1: Werkzeugmaschinenlabor WZL der RWTH Aachen

Source: Werkzeugmaschinenlabor WZL der RWTH Aachen, 2017

Located in the westernmost German side of the city of Aachen and at the borders with Belgium and the Netherlands, the Laboratory for Machine Tools and Production Engineering of RWTH Aachen is one of the most important technical research institutes of Germany, belonging to RWTH-Aachen University. The institute employs about 800 people and positively affects process optimization and technological industrial development in the manufacturing sphere with practical and innovative solutions. The research institute of the Aachen University was founded in 1906 and is headed by four professors, who cooperate to manage four core research chairs of the institute, as described below:

- **Prof. Dr.-Ing. Christian Brecher – Chair of Machine Tools:** this area encompasses the calculation and optimization of machine tools and handling systems, including all component parts, the metrological inspection and evaluation of production systems, drive technology, NC, PLC systems, process monitoring and machine

diagnostics, human-machine interaction, as well as control systems technology and automation.

- **Prof. Dr.-Ing. Robert Schmitt – Chair for Production Metrology and Quality Management:** the core areas of this research field include the development and optimization of measurement processes and equipment, production-integrated metrology, machine-oriented quality control loops, quality management systems, as well as knowledge, innovation and optimization management. Furthermore, quality management methods and computer-aided quality management are also the subjects of the chair's research.

- **Prof. Dr.-Ing. Thomas Bergs – Chair for Technology of Manufacturing Processes:** this research area covers the fundamentals of manufacturing technology, process analyses, process monitoring, process modeling and simulation as well as environmentally sound technologies.

- **Prof. Dr.-Ing. Dipl.-Wirt. Ing. Günther Schuh – Chair of Production Engineering:** this research area focuses on production planning issues. This includes core topics such as integrated process and product design, cooperative value creation, business modeling and system selection.

This final project work was held in the department of Prof. Dr.-Ing. Christian Brecher – Chair of Machine Tools, sector of Machine Tools, under the supervision of Florian Kneer, M.Sc. RWTH.

3 STATE OF THE ART

In this work, a distinction is made between the terms thermal, thermal-elastic, structural-mechanical and thermal-mechanical simulation. In the thermal simulation only a temperature field is generated, which in itself represents the result. The thermal-elastic approach determines the reversible deformation of the geometry by the temperature field, while in the structural-mechanical simulation, the reaction of the system by forces, moments and connecting elements is determined. The thermal-mechanical analysis combines the thermal-elastic and structural mechanical effects.

In an effort to put the investigation of ball screws thermal-mechanical behavior into context, the general structure of ball screws will be first discussed and then the thermal behavior modeling will be described along with friction influence.

3.1 Ball Screws Drivers

The patent of a ball screw system was first filed in 1931 and consequently changed the power screw industry ever since. In general, a ball screw consists of a screw and a nut system, both equipped with raceways, as well as the rolling elements, which separate the raceways of screw and nut system [4]. The nut rotation around its axis translates the nut in its axis direction since the screw grooves are continuously provided in a helical form. Namely, the screw is a mechanical element that converts a rotational motion into a linear motion. By providing rolling elements in between the screw shaft and the nut (grooves), the rolling elements roll into the grooves and change the sliding contact to rolling contact reducing the friction, as can been seen in Figure 2a [5].

In the case of a ball bearing system, its balls roll only in a circular groove, since the groove in the ball screw is helical. Its balls roll along the helical groove and could leave the ball nut unless they are rolled at a defined spot. Thus, it is necessary to change their path after they have reached a defined spot by guiding them, one after another, back to their “starting point” (formation of a circular path). The recirculating systems have this functionality.

When the screw shaft is rotating, as shown in Figure 2b, a ball at point (A) travels 2.5 turns of screw groove, rolling along the grooves of the screw shaft and the ball nut, and reaches point (B). Then, the ball is forced to change its pathway at the tip of the

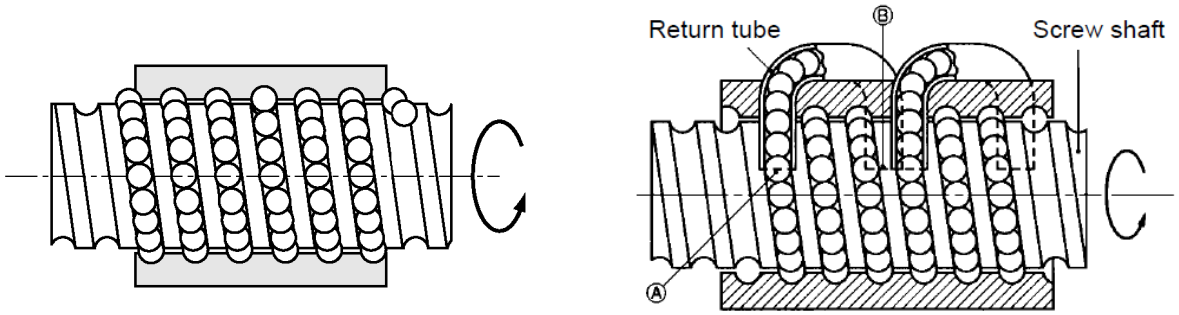

(a) Screw, Ball and Nut Contact (b) Ball Screws Recirculation System

Figure 2: Ball screw drivers

Source: NSK Ltd.

tube, passing back through the tube, until it finally returns to point (A). Whenever the nut strokes on the screw shaft, the balls repeat the same recirculation inside the return tube.

3.1.1 Preload and Stiffness of Ball Screws

One of the main characteristics of a ball screw is the ability to change its stiffness by defining different levels of preloading [6]. The aim of the preload force (Fa_0) is to create elastic deformations between the rolling elements and ball grooves on the nut and the screw shaft in order to prevent loss of ball contact (also know as backlash) and increase system axial stiffness and positioning accuracy [7].

Ball screws can use different preloading systems depending on the individual application. In Figure 3 it is illustrated a double nut spring preloading system. In those systems springs play the role of a damper and the spring force acts as a preload. Therefore, high-resolution positioning can be reached using preloading, which yields the following effects:

- reduction of the axial play between a screw shaft and a ball nut (lower backlash);
- minimization of the deformation caused by external forces (stiffness enhancement).

However, setting more preload than required increases stiffness, which results in more torque required for rotation and consequently increases heat generation due to the high friction forces [6].

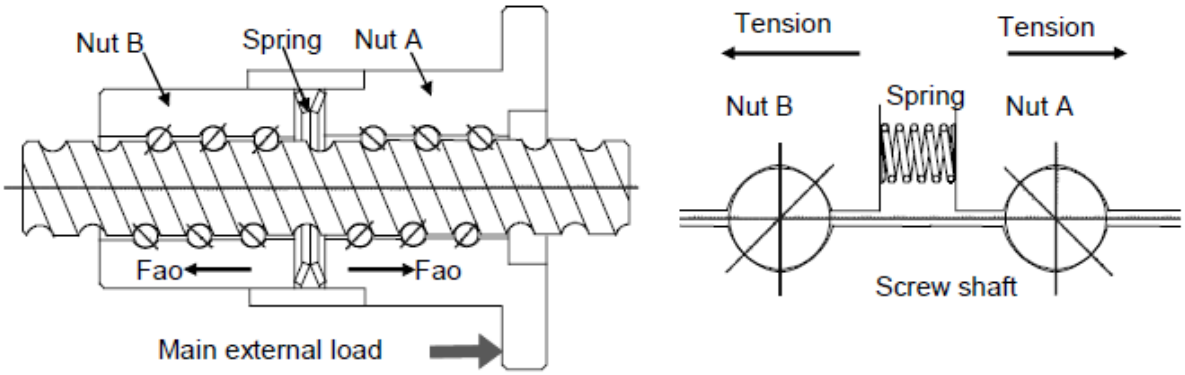

Figure 3: Double nut ball screw with spring preload system

Source: NSK Ltd.

3.1.2 Ball Screws Contact Characteristics

The contact characteristics of ball screws depend on its preload systems. Ball screws that do not have a preload system are called single nut ball screw and have 4 points of contact between the balls and the raceway grooves. Ball screws that have preload systems are called double nut ball screws and have 2 points of contact between the balls and the raceway grooves [5]. In this final project work a double nut screw with a preload system was used.

According to [8], the forces and moments acting on a ball in a two points contacts ball screw system can be represented in Figure 4a. The figure illustrates the position of a ball and the position of a normal Load Q, with relative rotation from the screw with an angular speed w and relative movement from the nut with an axial speed v.

The tangential forces on ball-race contact ellipses between the balls, the screw grooves and the nut are show in Figure 4b. Between ball, nut and screw act the following forces: hydrodynamic rolling forces FR, pressure forces FP, FPb and friction forces FS. Between the balls essentially acts FB.

In Figure 5b the moments which act on the ball and are generated on the contact ellipses are illustrated: MC and MER. MC represents the curvature friction and MER the moments due to the elastic resistance caused in the balls.

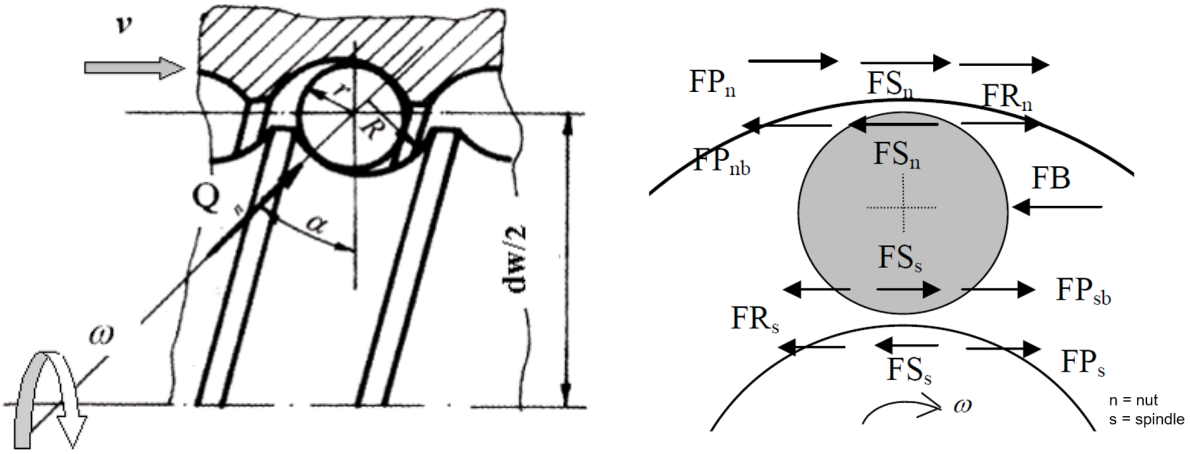

(a) Contacts between ball and the two races (b) Forces acting on the ball and on the two races

Figure 4: Tangential forces on ball-race contact ellipses

Source: A New Model to Estimate Friction Torque in a Ball Screw System [8]

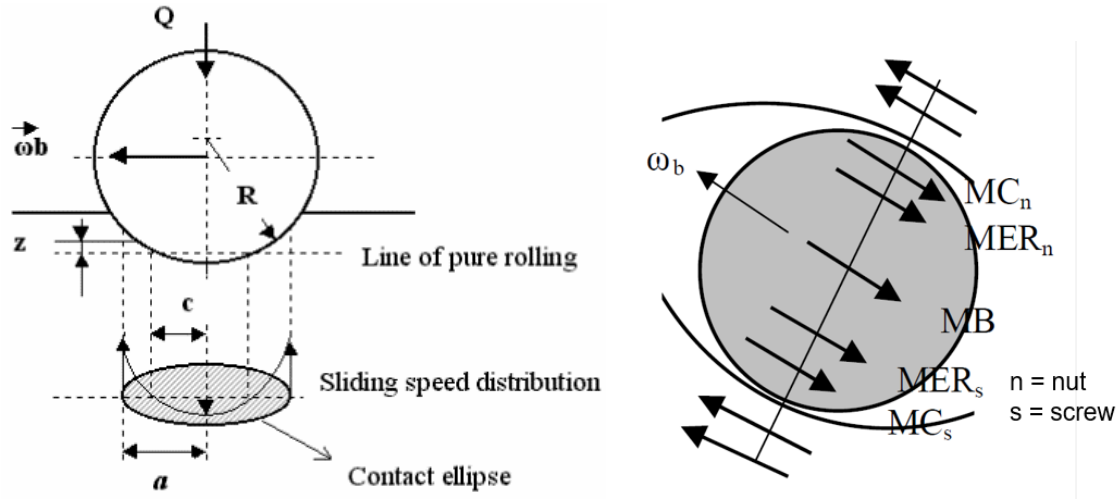

(a) Sliding speed distribution (b) Moments acting on the ball and on the two races

Figure 5: Moments on ball-race contact ellipses

Source: A New Model to Estimate Friction Torque in a Ball Screw System [8]

3.2 Ball Screws Thermal Modeling

In any mechanical system with relative movement heat is generated by friction [9]. Temperature distribution is commanded by heat input, heat conduction between elements and heat output. The distribution and balance of these heat sources will determine the thermal behaviour.

[2] proposed a thermal model to evaluate preload variations in double ball screws

systems, in the face of thermal variations caused by friction due to the relative movement of the nut in the screw. Due to its similarity to this final project work and since the model in [2] was experimentally validated, such model was used in this work.

3.2.1 Conduction Heat Transfer

Conduction is a heat transfer mode in which heat flows in a substance due to the exchange of energy among molecules having different levels of energy for being in regions with different temperatures. Heat conduction occurs due to the interaction among molecules in all substances, like solids, liquids, and gases. In 1822, J.B. Fourier proposed an empirical law to govern the heat conduction problem. Fourier's law (3.1) of heat conduction states that the heat flux, resulting from thermal conduction, is proportional to the negative local temperature gradient [10].

$$q = \frac{\dot{Q}}{A} = -k\frac{dT}{dx} \tag{3.1}$$

In Eq. 3.1, q is the heat flux [W/m^2] defined as heat flow per unit area perpendicular to the heat flow direction, and k [W/m K] is the thermal conductivity of the material, indicating the rate of heat transfer per unit area and per unit temperature gradient [10].

3.2.2 Convective Heat Transfer

Unlike conduction in fluids, which occurs due to the motion of molecules in a microscopic scale, the movement of fluids in a macroscopic scale can also transfer energy. Heat exchange from a solid surface to a moving fluid is called convection or convective heat transfer [10].

The convection process can be forced or can be free (natural). When the flow of the fluid is caused by an external factor, like a screw shaft rotation, the process is called a forced convection. Heat transfer by convection is called free or natural convection when there is no external forcing element and motion of the fluid is caused by density variations due to temperature difference [11]. Heat transfers by forced and free convection are schematically depicted in Figure 6.

The rate of heat transfer by convection is dependent on the geometry and temperature of the surface as well as the temperature, velocity, and thermal-physical properties

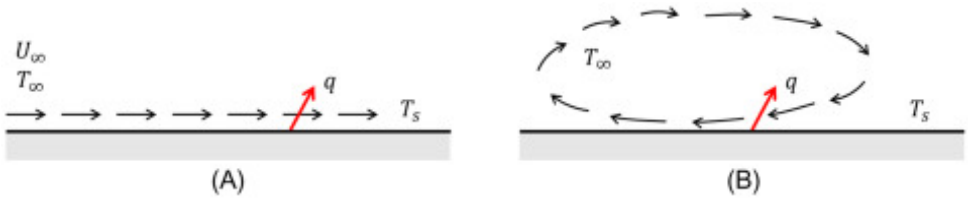

Figure 6: Schematic illustration of heat transfer by (A) forced convection and (B) natural of free convection. $T_s > T_\infty$.

Source: Nonlinear Systems in Heat Transfer [10]

of the fluid [12]. The rate of convective heat transfer from a surface at temperature T_s to a fluid at temperature T_∞ is given by:

$$q = \frac{\dot{Q}}{A} = h(T_s - T_\infty) \tag{3.2}$$

where h is the convective heat transfer coefficient. Eq. 3.2 is also known as the Newton's law of cooling and was first suggested by Isaac Newton to describe a typical convective cooling processing.

3.2.3 Radiation Heat Transfer

Differently from the previous two modes, heat transfer by means of radiation can occur without any medium. Radiation is transmitted by electromagnetic waves or photons caused by the changes of electronic configurations of an atom or molecule [13]. For thermal radiation, the amount of radiation emitted by a body is proportional to its absolute temperature raised to the fourth power multiplied by the Stefan-Boltzmann constant (σ) and an emissivity coefficient (ε), as modelled by the Stefan-Boltzmann law (3.3):

$$q = \frac{\dot{Q}}{A} = \varepsilon \cdot \sigma \cdot T^4 \tag{3.3}$$

3.2.4 Heat Generation

According to [2], in a ball screw system the primary contributors to heat generation are the rolling elements within the nuts and the screw. The heat input of these elements can be modelled as uniformly distributed surface heat fluxes in the thermal model.

The heat generation of the nut-screw coupling is composed of the fraction acting

on the nut and the heat fraction acting on the screw shaft as showed in Equation 3.4. In the model suggested by [2], these fractions are considered equally distributed. As shown in Figure 7, the screw surface heat flux is comprehended between the end of Nut 1 and the end of the working length, while for the nuts, the heat flux is directly applied to the nut raceways.

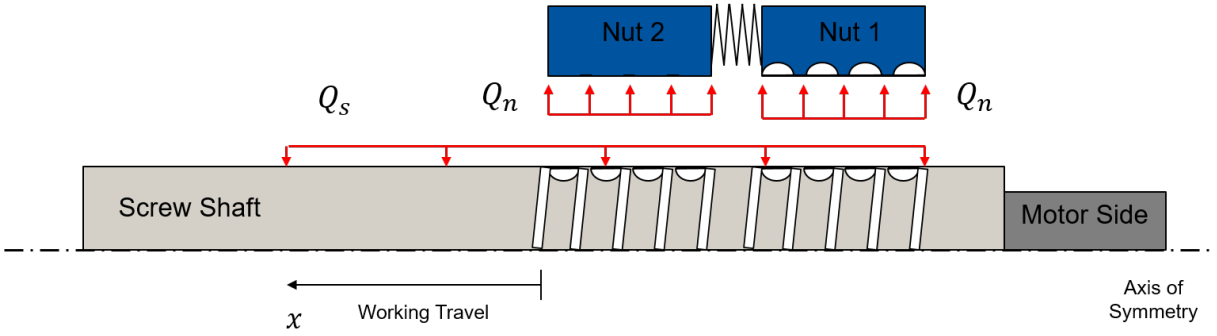

Figure 7: Thermal scheme of heat generation.

Source: original.

$$Q_{ns} = Q_n + Q_s \tag{3.4}$$

As shown in Equation 3.5, heat generation is the product between the angular speed ω and the frictional torque of the nut (Mr_n), which depends on the friction coefficient (μ), the sum of contact normal load (F_n) and the action radius (r_c) in Equation 3.6.

$$Q_{ns} = Mr_n \cdot \omega \tag{3.5}$$

$$Mr_n = F_n \cdot \mu \cdot r_c \tag{3.6}$$

3.2.5 Heat Diffusion

The heat is dissipated by radiation, convection and conduction. The convection heat dissipation transfers energy from the surfaces to the surrounding environment. Thus, according to [2], only the surfaces in contact with the air are defined as convective surfaces, as can been seen in Figure 8. Since the heat conduction occurs through solid elements, internal parts conduction and thermal conductance between contacting components must be taken into account, as shown in Figure 9.

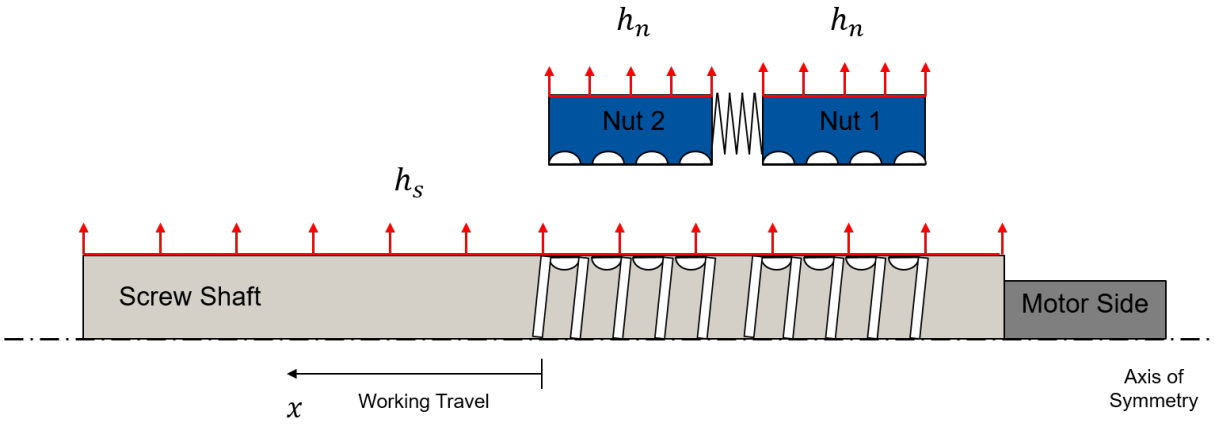

Figure 8: Thermal scheme of heat convection.

Source: original.

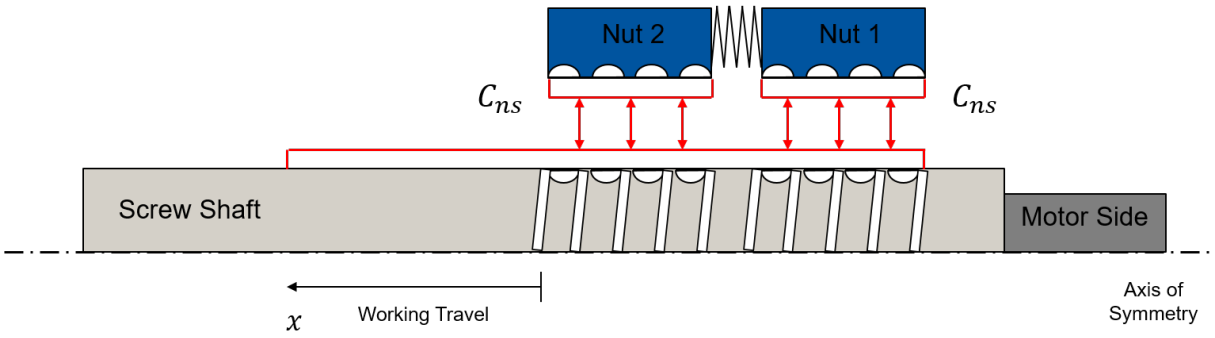

Figure 9: Thermal scheme of heat conduction.

Source: original.

3.2.5.1 Convection Coefficients

The convection coefficients are calculated considering whether the relative velocity between the surrounding air and the solid surfaces will generate free or forced convection [14]. Multiple correlations can be used depending on the solid shape and motion.

In the model suggested by [2], for the case of the screw shaft, it is considered a horizontal rod that rotates around its axial axis. Therefore, the linear relative motion of the outer surface shows that forced convection must be considered. The Reynolds number (Re) determines whether the air that flows on an external surface is laminar or turbulent, depending on the linear speed of the surface (s_{sur}) and the air viscosity (υ_{air}). Equation 3.9 shows the Nusselt (Nu) correlation, used for calculating the forced

convection coefficient h_{forced}. Pr and k_{air} are the Prant number and the air conductivity, respectively.

$$s_{sur} = \omega \cdot \frac{d_0}{2} \tag{3.7}$$

$$Re = \frac{s_{sur} \cdot d_0}{\upsilon_{air}} \tag{3.8}$$

$$Nu_{forced} = 0.664 \cdot Re^{0.5} + Pr^{0.33} \tag{3.9}$$

$$h_{forced} = \frac{Nu \cdot k_{air}}{d_0} \tag{3.10}$$

The nuts are also considered as horizontal rods, but in this case, the linear motion is the same as the linear speed of the table. The relatively slow motion suggests to consider free-forced combined convection (h_{comb}), as can be seen in Equation 3.11, where D_{nut} is the outer diameter of the nut body.

$$Nu^3_{comb} = Nu^3_{forced} + Nu^3_{free} \tag{3.11}$$

$$h_{comb} = \frac{Nu_{comb} \cdot k_{air}}{D_{nut}} \tag{3.12}$$

Remarking to the Nusselt number of the free convection case (Nu_{free}), the Grashof number (Gr) depends on the temperature difference between the surface (T_s) and the air (T_{air}), where β is T^{-1}_{air}. In this case, the Nusselt number is obtained using Rayligh number (Ra) and C and p constants obtained from the literature [15].

$$Gr = \frac{9.81 \cdot \beta(T_s - T_{air})D^3_{nut}}{\upsilon^2_{air}} \tag{3.13}$$

$$Ra = Gr \cdot Pr \tag{3.14}$$

$$Nu_{free} = C \cdot Ra^p \tag{3.15}$$

3.2.5.2 Conduction

Internal heat conduction through the components can be computed by a model derived by [2]. Nonetheless, the heat is conducted not only through continuous solids but through joints and contacting surfaces between components. The thermal conductance defined between the inner surface of the nuts and the outer surface of the screw shaft Figure 9 represents the heat transfers through the rolling elements and the lubricant.

3.3 Finite Element Analysis

An examination of the finite element analysis process first requires a look back at the history of the method.

The method of representing a domain as a collection of discrete parts can be traced back as far as ancient mathematicians in their estimations of the value of π to the accuracy of nearly 40 significant figures by representing a circle as a polygon of a very large but finite number of sides [16]. In 1851, Schellback discretized a surface into finite right triangles and wrote a finite difference expression to solve for the total area in an endeavor to determine the surface of minimum area confined by a closed curve in space [17]. These examples show early applications in which bodies were discretized into "finite elements" to solve problems.

In the field of thermal systems analysis, it is difficult to analytically solve the heat transfer laws for complex geometries. For this reason, discrete numerical solution methods have been used to solve thermal problems, mainly the finite difference method and the finite element analysis method. In this work, the latter approach is used.

Finite element analysis (FEA), also known as the finite element method (FEM), is a method for numerical solution of field problems. A field problem requires the determination of a spatial distribution of one or more dependent variables such as heat and mass transfer and fluid flow problems in oil and gas industries. Mathematically, a field problem is described by differential equations or by an integral expression [18]. At its basis, FEA is a numerical method to solve engineering field problems by dividing a domain into smaller finite sub domains, each of which acts as an individual element over which differential

equations or integral expressions are applied and an approximate solution is given [19]. Elements are connected at points called nodes. The assemblage of elements is called a finite element structure, as can been seen in the example in Figure 10.

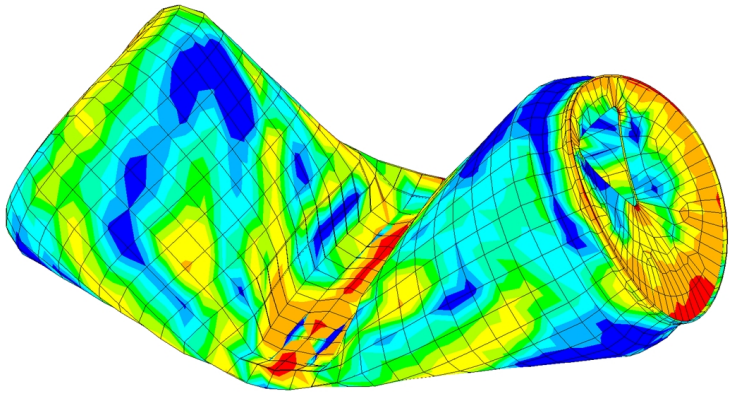

Figure 10: Beer can surface model constructed of 2D shell elements

Source: Recoil Engineering © 2016

According to [18], the basic method by which a problem is solved using FEA can be broken down into several steps, namely:

I **Classification:** in this step it is necessary to identify the physical phenomena involved, whether the problem is time-dependent or time independent.

II **Modeling:** an analytical method is applied to model a problem. A model for analysis can be devised after the physical nature of the problem has been understood. A geometric model becomes a mathematical model when its behavior is described, or approximated, by selecting differential equations and boundary conditions.

III **Discretization:** a mathematical model is discretized by dividing it into a mesh of finite elements. Thus a fully continuous field is represented by a piece-wise continuous field defined by a finite number of nodal quantities and simple interpolations within each element.

An illustration of these steps can been seen in Figure 11.

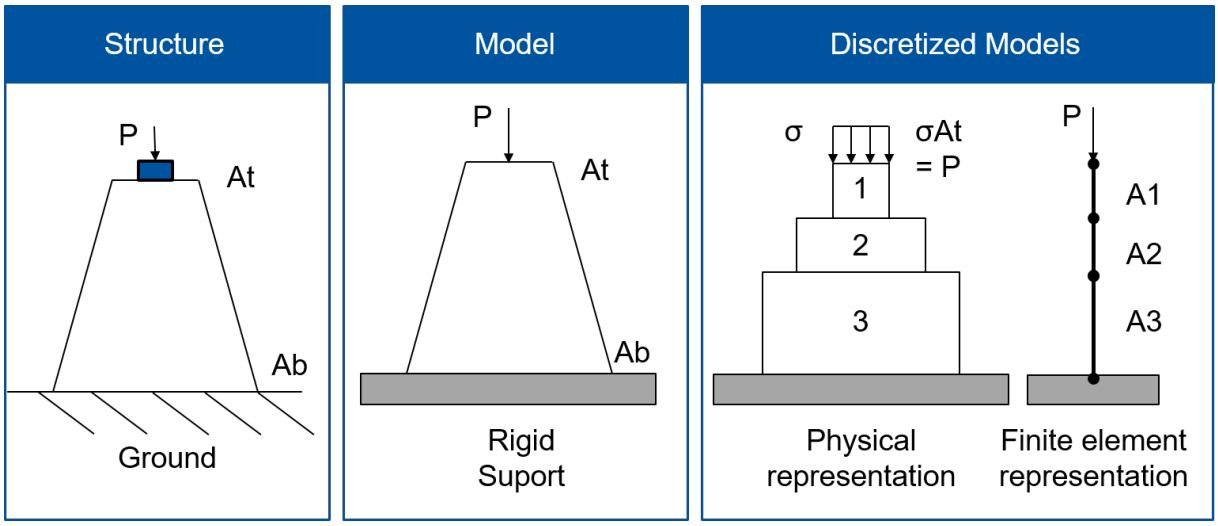

Figure 11: Steps in modeling a tapered support post using and FEA.

Source: Concepts and applications of Finite Element Analysis [18]

3.4 Existing Calculation Models for Ball Screw Systems

In the following, a briefly discussion about existing solutions for the simulation of ball screws systems is presented.

3.4.1 MTPlus

At the WZL from RWTH Aachen University, a simulation software for rolling elements characteristics and structure stiffness calculation in ball screws systems is being developed. Its calculation approach was originally developed for spindle bearing systems [20].

The rolling elements characteristics calculation is combined with a FE model of beam elements to obtain the state condition of the rolling elements. This is characterized by the displacement of the nut and screw shaft and the stiffness change. Angular speed, preload and the influence of external loads such as static forces in the axial direction as well as torques are taken into account. Based on the calculated state conditions and operating points, the static and dynamic behavior of the ball screw system can be investigated.

The rolling element contact model is established based on a method for angular contact ball bearing made known by Tüllman [21]. The contact forces are calculated by evaluating the current position of the rolling elements and the grooves. Therefore, the

rigid body overlap between the contacting bodies is determined and the contact forces are calculated using Hertzian theory. Under the assumption that all forces acting on the rolling element must be in quasi-static equilibrium, the positions of the rolling elements are calculated in an iterative process. The necessary displacements q, along the degrees of freedom, are determined by solving the following linear system of equations:

$$F = K \cdot q \iff q = K^{-1} \cdot F \tag{3.16}$$

Here, F describes the sum of forces on the rolling element, while K is the stiffness matrix. To determine matrix K, the rolling element is displaced along its degrees of freedom. By dividing the change of forces and the infinitesimal displacements, the stiffness value for both the direct and cross stiffness values are given.

In the case of a ball screw, the mathematical model must consider the lead angle's influence on the contact forces. Due to the lead angle φ, shown in Figure 12, the contact plane is inclined.

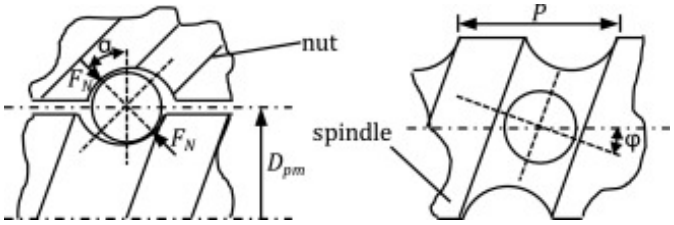

Figure 12: Geometry parameters

Source: Modelling of ball screw drives rolling element contact characteristics [4]

Therefore, the axial component F_{ax} of the contact normal force F_N does not only depend on the contact angle α:

$$F_{ax} = F_N \cdot \sin(\alpha) \cdot \cos(\varphi) \tag{3.17}$$

Figure 13 shows the calculation process. It can be divided in the following steps:

1. the system, including geometry and boundary conditions, must be set;
2. the system matrices for the beam elements are created and the reference position with no load for each rolling element model is determined;

3. different calculation jobs are executed successively. At each calculation job, the differential equation is solved iteratively, while in each iteration step the stiffness of the rolling elements is updated using a numeric analytical model.

The calculation results are the rolling element characteristics, such as the contact pressure, load angle and the normal forces, and the system characteristics, such as the elastic deformation of the nut and screw or the load distribution of the rolling element contacts.

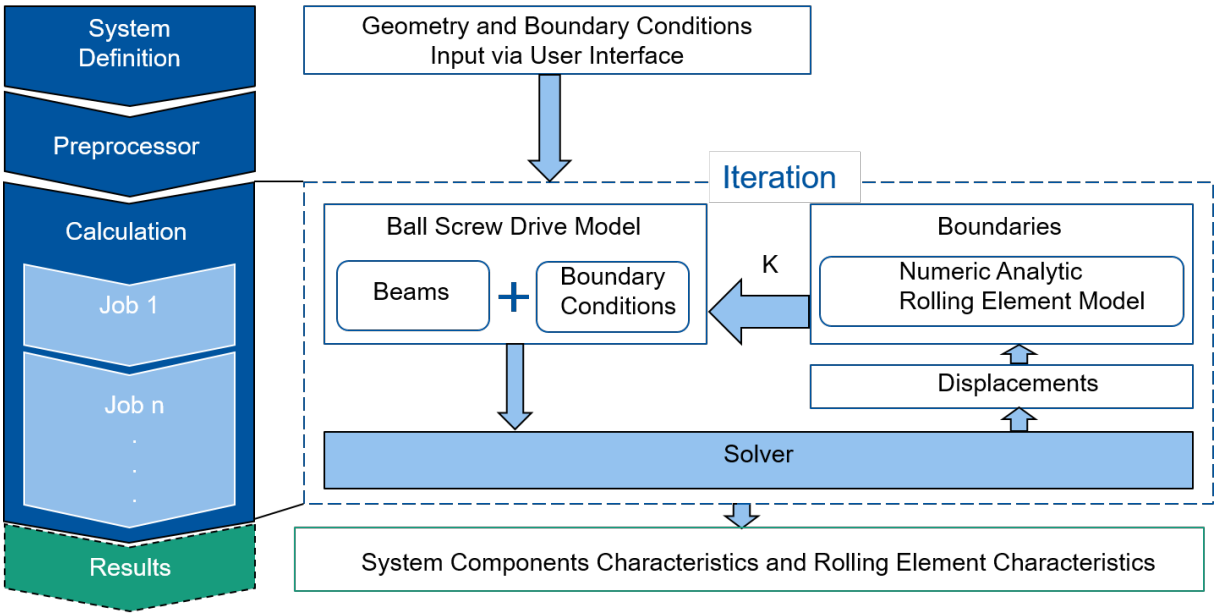

Figure 13: MT Plus calculation process

Source: original

3.4.2 MESYS Software for Mechanical Engineering

MESYS AG is an engineering company in Zurich Switzerland that develops software for technical calculations in mechanical engineering. The MESYS software for ball screws simulation is capable to calculate load distribution as a result of axial and radial loading and tilting moment. It uses the Hertzian contact stress theory as MTPlus. The load distribution is calculated under the assumption of rigid screw and rigid nut by considering the contact stiffness of the balls. A parameter variation allows an automatic combination and variation of input values and a graphical representation of the results.

The software also allows that influences of thermal and elastic expansions in radial and axial direction are taken into account [22].

By each simulation calculation the software can output load distribution between rolling elements, reaction forces and moments and displacements with rotations, contact pressure for each rolling element contact and contact angles according to the axial position of the ball.

4 THERMAL-ELASTIC BALL SCREW MODEL

The thermal-elastic ball screws simulation, which is one of the results of this work, was inserted into the simulation software MTPlus developed at the WZL. It was originally created to structurally simulate ball screw systems by means of beam cross-linking elements. The simulation software major emphasis is on a numerical, analytical rolling elements and components structure displacements calculation.

The thermal simulation calculation approach in conjunction with the structural mechanical simulation can been seen in Figure 14. First, the system, including geometry and boundary conditions, must be defined. Second, the system is discretized, matrices for the beams are created and the reference position with exactly no load for each rolling element model is determined. In a third step, different calculations jobs are executed successively. Within a calculation job, the differential equation is solved iteratively, while in each iteration step the stiffness of all rolling elements is updated using the numeric analytical model.

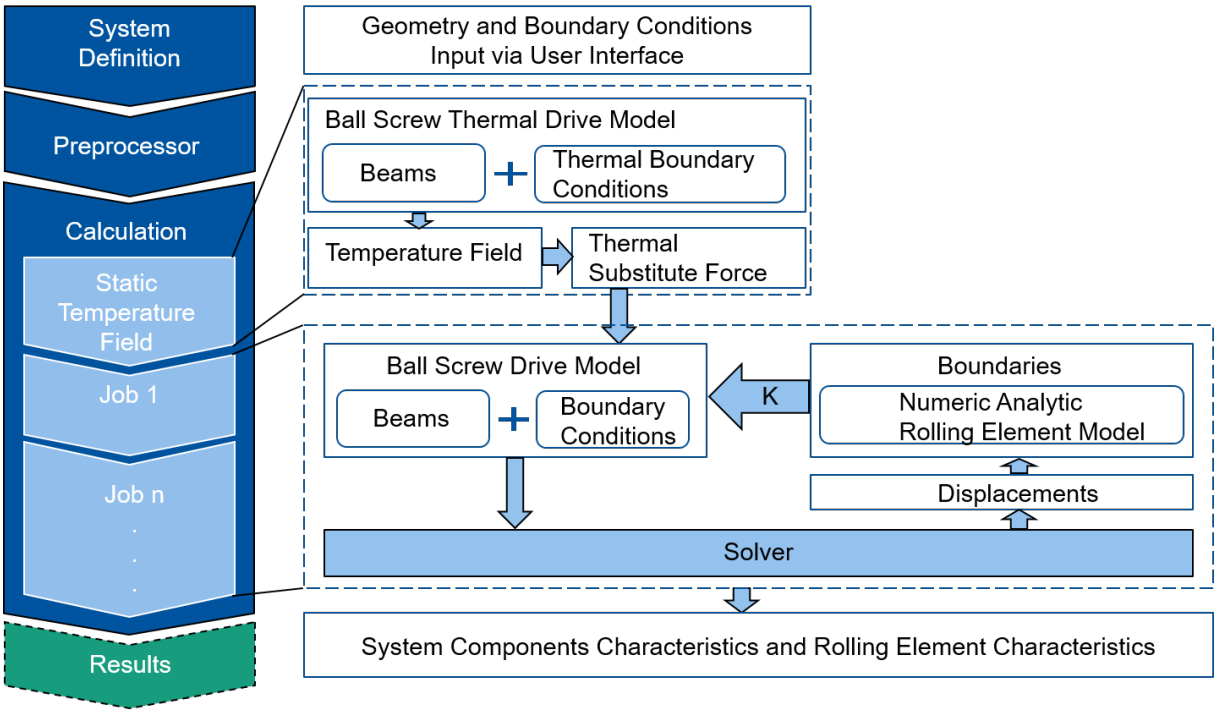

Figure 14: Thermal-Elastic simulation approach

Source: original.

To determine the temperature field, the thermal boundary conditions defined in the

first step and the discretized model created by the Preprocessor were used. Afterwards, the calculated temperature field is converted into thermal equivalent forces and transferred to the mechanical structural solver. The bearing calculation is updated within the classical calculation procedure with the axial displacements of the screw shaft and nuts. The calculation results can be visualized and evaluated by means of graphs.

In order to implement the temperature field calculation, MTPlus was extended in several locations. In the main user interface, new interface windows had to be created and existing ones had to be added with new options to enter the properties of the thermal boundary conditions.

4.1 MTPlus User Interface

In the MTPlus user interface, the geometry can be specified in the form of rotationally symmetrical forms. These can be combined with rolling elements, linear elastic connections and constraints. Further adjustments are possible for the individual elements, such as spring stiffness in the linear elastic connections and a preload force. In addition to the geometrical configurations, it is also possible to specify the operating conditions of the constraints, such as the degrees of freedom to be considered in structural mechanical simulation.

Figure 15 shows the MTPlus interface. On the left side there is a list of all components that are mounted in the ball screw model to be simulated. Just below there are buttons that allow the creation of new components and also the possibility to configure the existing ones. On the right side there is a graphic representation of the system.

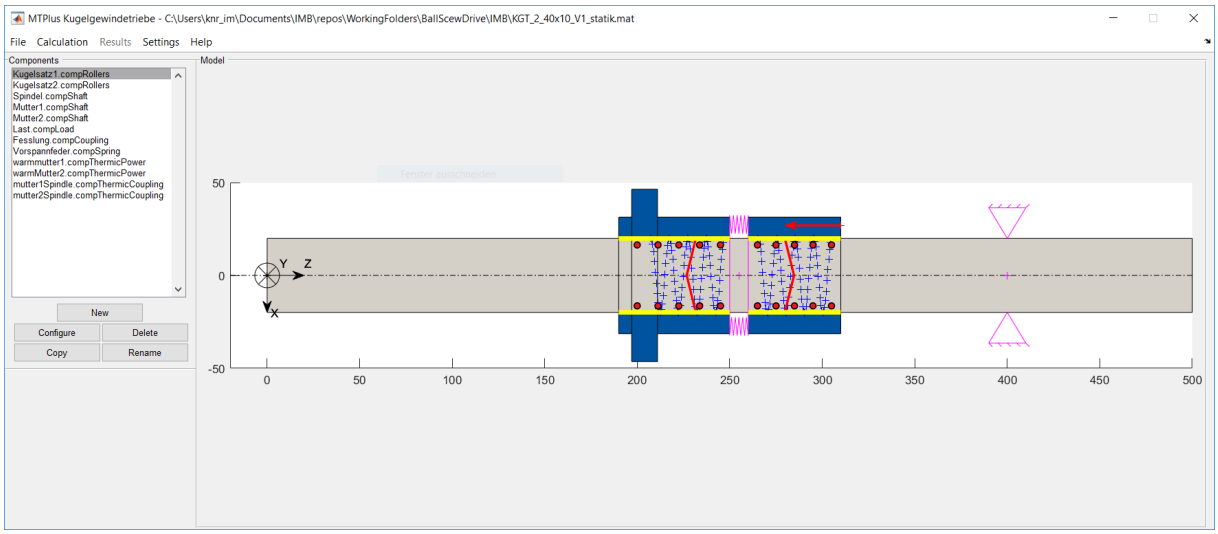

Figure 15: Thermal-Elastic MTPlus user interface

Source: original.

Figure 16 shows the individual components used to portray a ball screw model. The components shown have been created in the course of this work, such as heat sources and thermal connections.

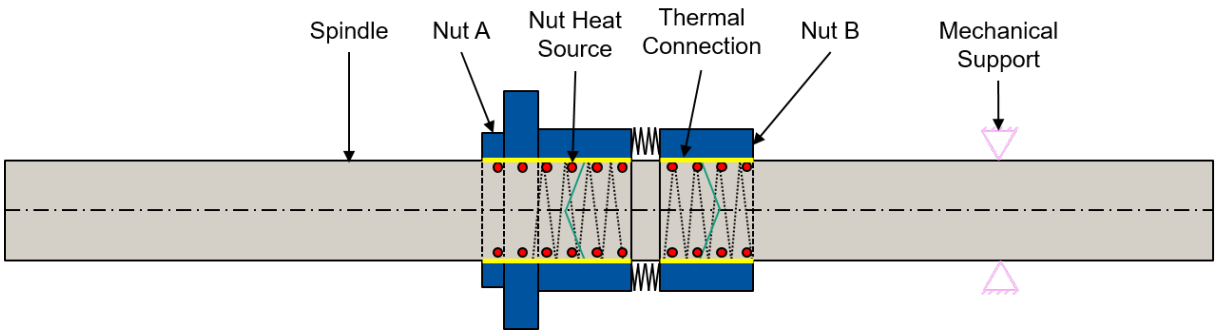

Figure 16: Thermal-Elastic MTPlus components

Source: original.

The components of the heat source are inserted into the system through an axial and radial position as well as a width. These simulation components were created to represent the amount of heat generated between the product of the angular speed and the friction torque showed in Equation 3.5. The thermal connection components also receive the same position and width parameters, on the other hand, their function is to allow the mechanical components of the model to have a thermal transfer rate. This is necessary, for example, to model the conduction heat transfer between the nuts and the screw shaft.

Thermal bonding elements must have a thermal transfer coefficient.

4.2 Ball Screw Geometry Discretization

The input geometric data and boundary conditions must be transferred to the simulation and then be processed. Using FEA it is first necessary to discretize the geometry with finite elements, defining nodes, their quantity (degrees-of-freedom, DOFs), numbering, element numbering, and element topology (which nodes define the element). Thus, it becomes possible to configure and solve approximation functions for each discretized element. Since the geometry representation in MTPlus is with only right angle elements, it becomes easier to discretize it with rectangular, rotational symmetric elements.

After discretizing the geometry as a one-dimensional beam model around the screw shaft axis for the existing mechanical parts, a separate discretization is processed for the thermal components, whic is illustrated in Figure 17.

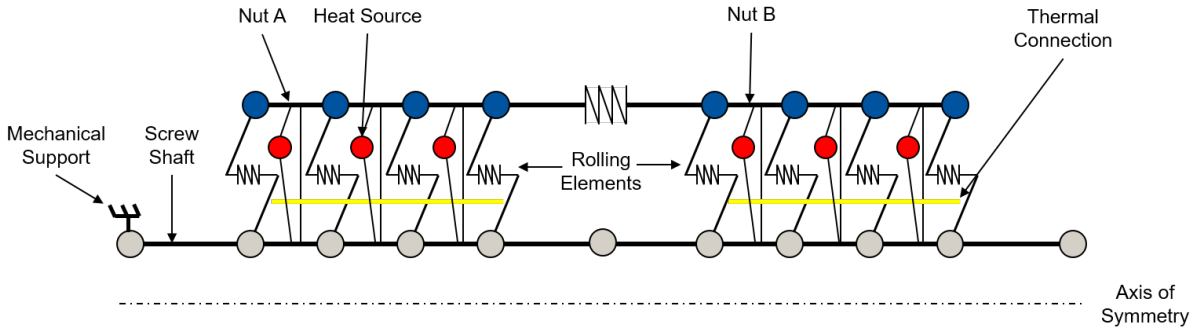

Figure 17: MTPlus discretization with thermal components

Source: original.

For the discretization of heat source components, their overall width shall be divided and limited to the elements generated by the first discretization. An algorithm then runs throughout the discretized system and identifies which elements are connected to the heat source and which elements are to receive a lot of heat. The thermal connection performs essentially the same algorithm, except that it always identifies two elements that are connected between a thermal connection component and defines a coefficient of thermal exchange between them. An illustration can be seen in Figure 18.

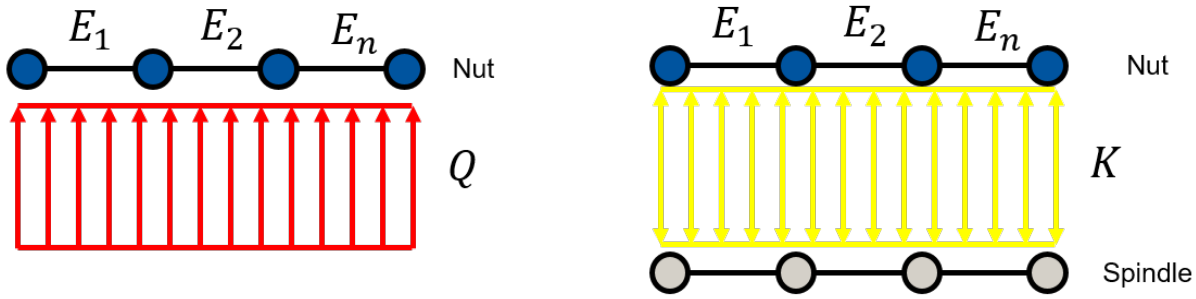

Figure 18: Thermal sources and connections discretization illustration

Source: original.

4.3 Temperature Field Calculation

Since MTPlus is based on jobs calculation, the temperature field was also implemented as another job inside the solver class from the simulation software. The temperature field calculation consists of setting up and solving partial differential equations. To this end, a strong formulation for heat conduction must be set up. Figure 19 shows the temperature field inside an arbitrary body and the heat flux across sides of a differential element.

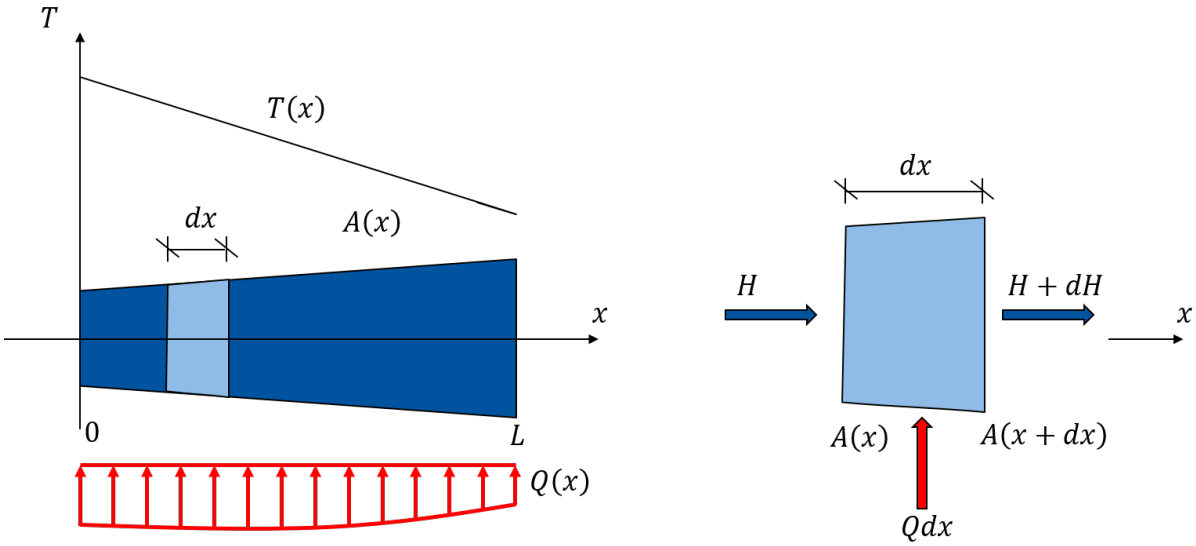

Figure 19: Temperature field and heat flux through sides of a plane differential element

Source: original.

Then the net rate of heat flow into a differential element of unit thickness is:

$$H + Qdx = H + dH \Rightarrow \frac{dH}{dx} = Q \tag{4.1}$$

Inward heat flow produces an increase of stored energy, specifically $c\ \rho\ \dot{T}$. Hence

$$Q - \frac{dH}{dx} = \rho \cdot c \cdot \dot{T} \tag{4.2}$$

and by definition:

$$H = A \cdot q \tag{4.3}$$

using Fourier's law 3.1 of heat conduction:

$$\frac{d}{dx}\left(Ak\frac{dT}{dx}\right) + Q - c\rho\dot{T} = 0,\ 0 \leq x \leq L \tag{4.4}$$

Where:

A = area
k = material thermal conductivity
Q = heat supply
ρ = material density
c = material specific heat capacity

Regarding the FE calculation, there are several applicable FE formulations. For this work, the Solid Bodies equations jointly with the compact statements provided by a functional and the notation used in Equations 4.5 were used [18]. Equations for solids are obtained by direct extension of the foregoing arguments. The equations can be written in matrix format using the following notation.

$$\{\partial\} = \begin{Bmatrix} \partial/\partial x \\ \partial/\partial y \\ \partial/\partial z \end{Bmatrix} \qquad \{T_\partial\} = \begin{Bmatrix} T_x \\ T_y \\ T_z \end{Bmatrix} \qquad \{\mu\} = \begin{Bmatrix} l \\ m \\ n \end{Bmatrix} \tag{4.5}$$

where l, m and n are direction cosines of a normal to the boundary. Further let $[k]$ be a square matrix DOFxDOF. Thus, for a solid body in rectangular Cartesian coordinates,

$$\{\partial\}^T ([k]\{T_\partial\}) + Q - c\rho\dot{T} = 0 \tag{4.6}$$

$$f_B = \{\mu\}^T [k] \{T_\partial\} \tag{4.7}$$

in which, the Equation 4.6 is the governing equation and the Equation 4.7 is the boundary conditions, for example, $f_B = h(T_{fl} - T)$ for a convection condition with T on boundary S for the solid surface.

The functional is represented by Equation 4.8 where, in the latter integrals, T is evaluated on boundary S and V, being those for geometry surface and volume.

$$\Pi = \int_V \left(\frac{1}{2} \{T_\partial\}^T [k] \{T_\partial\} - QT + c\rho T\dot{T} \right) dV - \int_S \left(f_B T + hT_{fl}T - \frac{1}{2}hT^2 \right) dS \tag{4.8}$$

To express T in an element in terms of element nodal temperatures T_e the Equation 4.8 becomes, for one element:

$$\Pi_e = \frac{1}{2} \{T_e\}^T \Big([k] + [h] \Big) \{T_e\} + \{T_e\}^T \Big([c] \Big\{ \dot{T_e} \Big\} - \{r_B\} - \{r_h\} - \{r_Q\} \Big) \tag{4.9}$$

Addition of element contributions Π_e provides Π of the assembled structure. Assembly implies the usual expansion of element arrays to the structure size, so that the array global temperatures $\{T\}$ replaces element arrays $\{T_e\}$. Thus the following FE equations are obtained, in which assembled arrays are denoted by upper case letters.

$$\begin{cases} [C] [\dot{T}] + [K_T] \{T\} = \{R_T\} \\ [C][\dot{T}] = 0 \\ [K_T] = [K] + [H] \\ \{R_T\} = \{R_B\} + \{R_H\} + \{R_Q\} \end{cases} \tag{4.10}$$

In this work only a steady-state temperature field was considered. This is characterized by the fact that there is no temporal change of the temperature.

The matrix $[K_T]$ consists of the sum between the heat conductivity matrix $[K]$ and the boundary convection and radiation matrix $[H]$. The vector $\{R_T\}$ summarizes the heat flux vector at the geometry surface $\{R_B\}$, the boundary convection vector $\{R_H\}$ and the heat generation vector $\{R_Q\}$.

To arrive at the global Equation 4.10, an element matrix and a vector must be set up for each element. The global equations system is then obtained as the composition

of each element equations system. Since the FEA uses a discretized geometry network, in which only the temperatures $\{T\}$ are determined at the nodes, the temperature T in Equation 4.11 at any point within the element is obtained through interpolation using the shape functions $\lfloor N \rfloor$.

$$T = \lfloor N \rfloor \{T\} \tag{4.11}$$

The linear shape functions for a two-node beam element used in the temperature field calculation are shown in Figure 20. The element dimension is L. Also, the global coordinate system x, T, are introduced. The shape functions N_i to N_j are combined in the line vector $\lfloor N \rfloor$ and correspond to the shape function for a single element mentioned at the Equation 4.11. Thus, the shape functions are standardized in each element on the nodes for which they are set up.

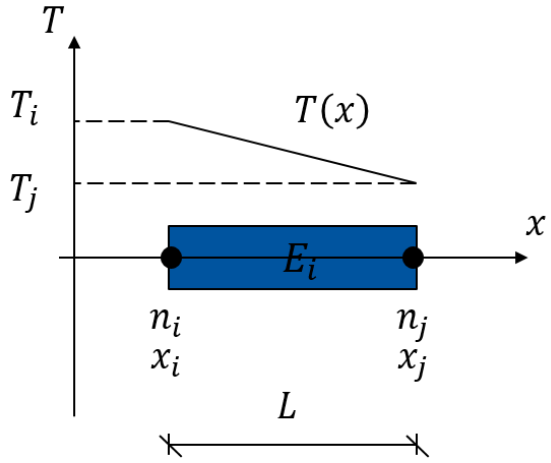

Figure 20: Linear variation of temperature on E_i Finite Element

Source: original.

$$\begin{cases} N_i = -\frac{1}{L}(x - x_j) \\ N_j = \frac{1}{L}(x - x_i) \\ \lfloor N \rfloor = \lfloor N_i \, N_j \rfloor \end{cases} \tag{4.12}$$

With regard to obtaining the temperature gradients, the Equation 4.11 is calculated according to the global coordinate system x, T.

$$\left\{ \frac{\partial T}{\partial x} \right\} = \left[\frac{\partial N_i}{\partial x} \quad \frac{\partial N_j}{\partial x} \right] \left\{ \begin{matrix} T_i \\ T_j \end{matrix} \right\} = [B] \{T\} \tag{4.13}$$

Using the $[B]$ gradient matrix definition, the heat conductivity matrix $[K]$ from Equation 4.10 can be calculated for a single element as follows. For an isotropic substance, the $[k]$ matrix becomes a scalar.

$$[K] = \int_V [B]^T [k][B]\, dV \tag{4.14}$$

Regarding the calculation of the thermal boundary conditions of the heat convection and heat radiation, the matrix [H] must be set up for the geometry edges where the heat transfer occurs. For this purpose, the Equation 4.15 is set up for each single element surface of the network and summed to the heat stiffness matrix, as shown in Equation 4.10.

$$[H] = \int_S \lfloor N \rfloor^T \lfloor N \rfloor\, h\, dS \tag{4.15}$$

Since Equation 4.4 describes a thermal equilibrium, the corresponding heat flow generated by the environment and the heat generated by the friction between the mechanical components must also be taken into account. With this purpose, the vectors $\{R_H\}$ and $\{R_Q\}$ have to be determined. This is described by the Equations 4.16 and 4.17, where T_{fl} is the ambient fluid temperature and Q is the heat source power.

$$\{R_H\} = \int_S \lfloor N \rfloor^T h T_{fl}\, dS \tag{4.16}$$

$$\{R_Q\} = \int_V \lfloor N \rfloor^T Q\, dV \tag{4.17}$$

4.3.1 Global System of Equations

Once the matrix and the solution vector have been set up for each individual element, the system of equations must be set up for the entire system. The assignment between the individual equation system and the overall system takes place via a row and column indexing, in which the node number of the overall system forms the index. The same method is also used for the solution vector.

4.4 External Temperature Field

Considering that MTPlus uses static 1D beam elements which cannot capture the entire thermal dynamic behavior expressed for ball screws systems, an external temperature field simulation was developed. Its purpose is to determine the partial stationary

operating point of the thermal-mechanical ball screw system during machining processes or bench tests.

For the external simulation, a ball screws CAD model with contact definitions was built and networked using Ansys Workbench. From Ansys, the model is exported using APDL scripts and executed in an external Matlab simulation program. Afterwards, the simulation is performed by the MTPlus. For that, the external thermal simulation three-dimensional temperature field must be reduced to the beam model used in MTPlus. The three-dimensional temperature field reduction is shown in Figure 21. In the figure the three-dimensional temperature field is shown at the top in the cross-section and the beam network used in MTPlus-Thermo is shown below. During the conversion, a cutting plane is created for each node from the beam model, which is perpendicular to the screw axis. For clarity, not all of these section planes are shown in Figure 21. In the following, each of the components is formed independently of one another a mean temperature. For this, the FE elements of the three-dimensional mesh are cut with the cut edges. For the elements lying in the cutting plane, the size of the cut surfaces and the temperature on the cutting plane are determined. Of all the elements in a cut plane of a component, an average temperature is formed, which is weighted by the size of the cut surface. According to this principle, a temperature is assigned to each node of each beam.

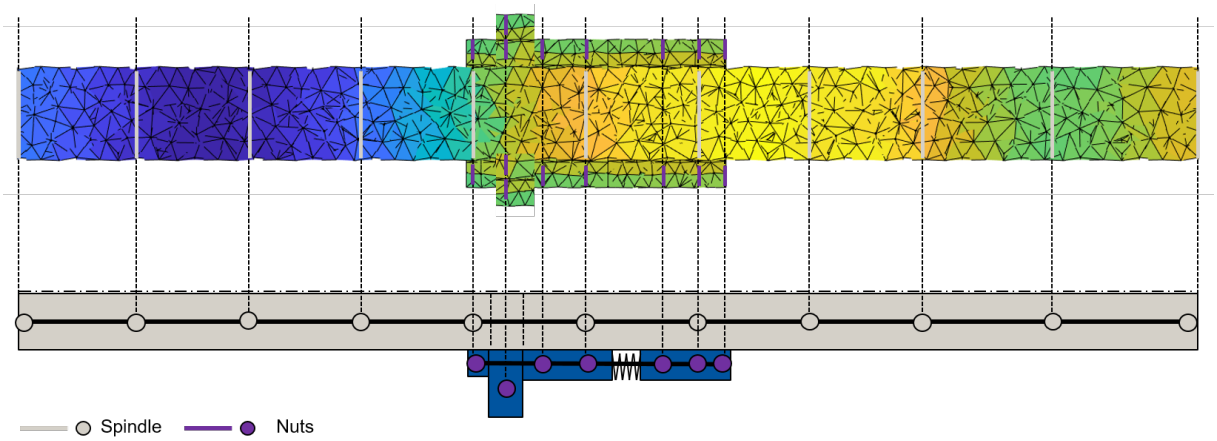

Figure 21: Temperature field reduction

Source: original.

The temperatures are then inserted into the MTPlus-Thermo simulation. Here, the thermal equivalent forces are determined and transferred to simulation calculation. The procedure is analogous to the newly implemented simulation and is described in the

section 4.5. The external simulation working flow is illustrated in the Figure 22.

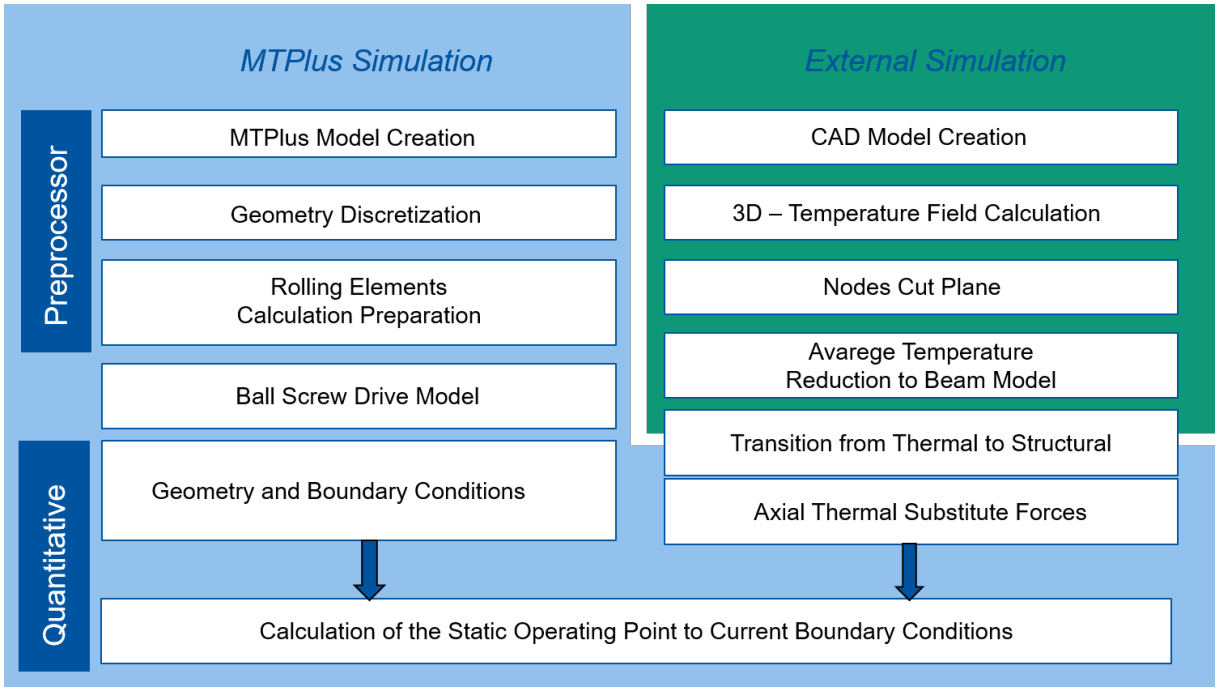

Figure 22: External simulation with MTPlus process work flow

Source: original.

An alternative to the presented approach would be the implementation of a thermal-elastic solver in the external temperature field calculation. This makes it possible to use the full, three-dimensional temperature field for the displacements determination. Thus, the radial displacements can be taken into account, giving a comprehensive picture of the thermal effects on the ball screw. All of the verified calculation methods of MTPlus for calculating the static behavior of the ball screw systems must be used to reduce the beam model in MTPlus. One option is using the thermo-elastic effects deformed geometry as starting geometry for MTPlus. It should be noted, however, that the material characteristics (eg modulus of elasticity, sliding modulus, density) must be adjusted accordingly.

4.5 Structure Model Integration

Since MTPlus is a structural stiffness simulation software, it uses forces and mechanical supports as boundary conditions. Thereby, the ball screw's temperature field must be converted into load boundary conditions. This is done in the form of thermal forces and strains on the rolling elements. Since the mechanical calculation of MTPlus

uses a beam model, only the axial change of the components is necessary for axial stiffness calculation. In addition, due to the calculated temperature field, no moments arise because the field is assumed to be rotationally symmetrical.

With the one dimensional temperature field, an equivalent thermal force is calculated using Equation 4.18

$$F_{T,x} = \alpha \cdot A_x \cdot E \cdot \Delta T_x \tag{4.18}$$

Where:

$F_{T,x}$ = thermal equivalent force in axial position x
α = material thermal expansion coefficient
A_x = cross section area in position x
E = elastic coefficient module
ΔT_x = difference between the reference temperature and the axial temperature at the position x

However, the thermal equivalent force is not fully inserted in the calculation, as it makes the rolling elements calculation unstable and can not usually be solved. Instead, the replacement force is divided into several increments of equal size, which are entered individually into the simulation, making the simulation slower but, on the other hand, stable.

5 EXPERIMENTAL SETUP

Experimental investigations on a ball screw were used to validate the calculation methodology. The experiment arrangement consists of two tables moved by two different double nut-ball screws parallel to each other. Between these two tables there are two load cells, separated in two sides, with one load cell equally spaced on each side. Inside one of the tables there is also two hydraulic pistons (actuators) equally spaced on each side in the same position of the load cells. The two double nut-ball screws are coupled as well to two different servomotors controlled by a programmable logic controller (PLC). Moreover, there are two displacement sensors positioned in front the bench ball screw. The schematic setup is shown in Figure 23.

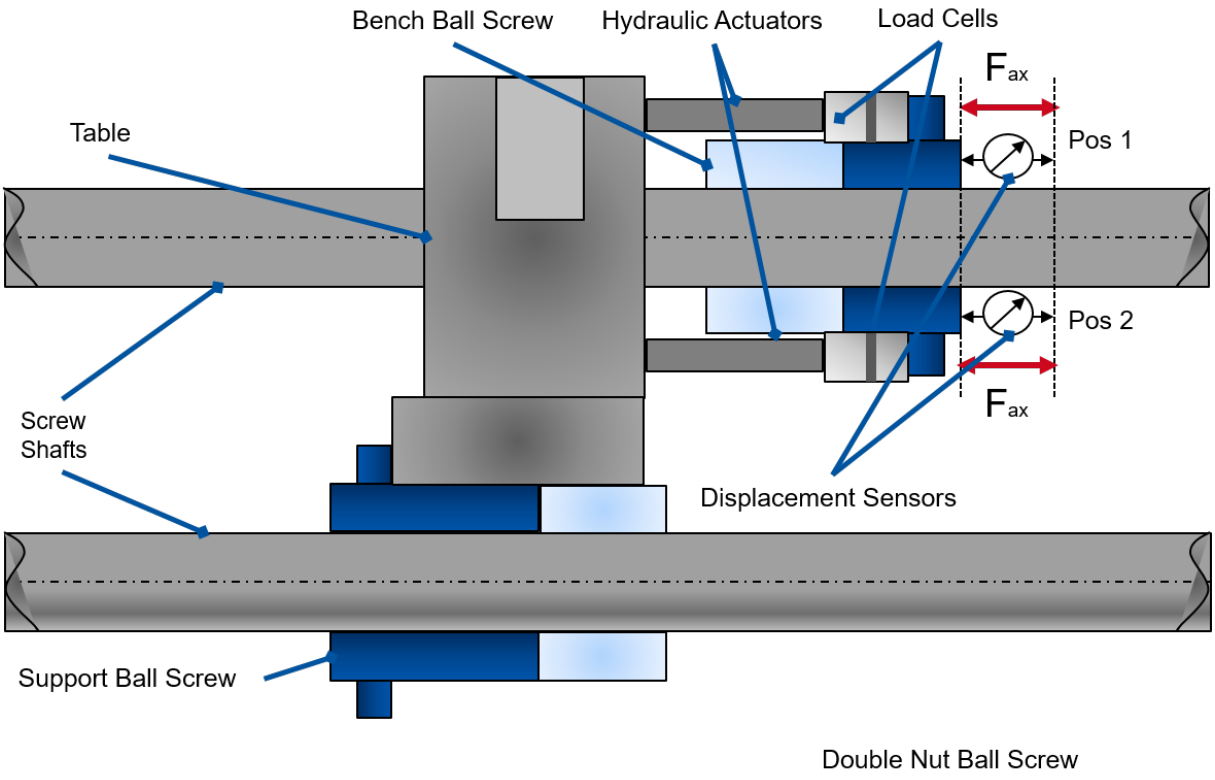

Figure 23: Setup schematic from the experiment

Source: original.

The experiment operation movement is similar to a pendulum. Each ball screw rotates in opposite directions, going back and forth to a pre-defined distance or position, repeating the movement until it reaches a predefined loop value. By that, the hydraulic actuators are activated to generate an axial force in the opposite table. The experiment

also has an integrated acquisition system for the load cells, pressure sensors, displacement sensors and torque sensors.

Figure 24 shows the main flow signals between the experiment, control and acquisition systems. The test begins with the definition of a final position in which the support and bench ball screws have to reach, but each in opposite directions. Thus, the PLC sends to the servo controllers the set position, these then starts to control the servo motors. Simultaneously pressure data, force and displacement are acquired by the acquisition system. The user also has the possibility to act on the force provided by the hydraulic actuators, setting a reference pressure for the pressure controllers.

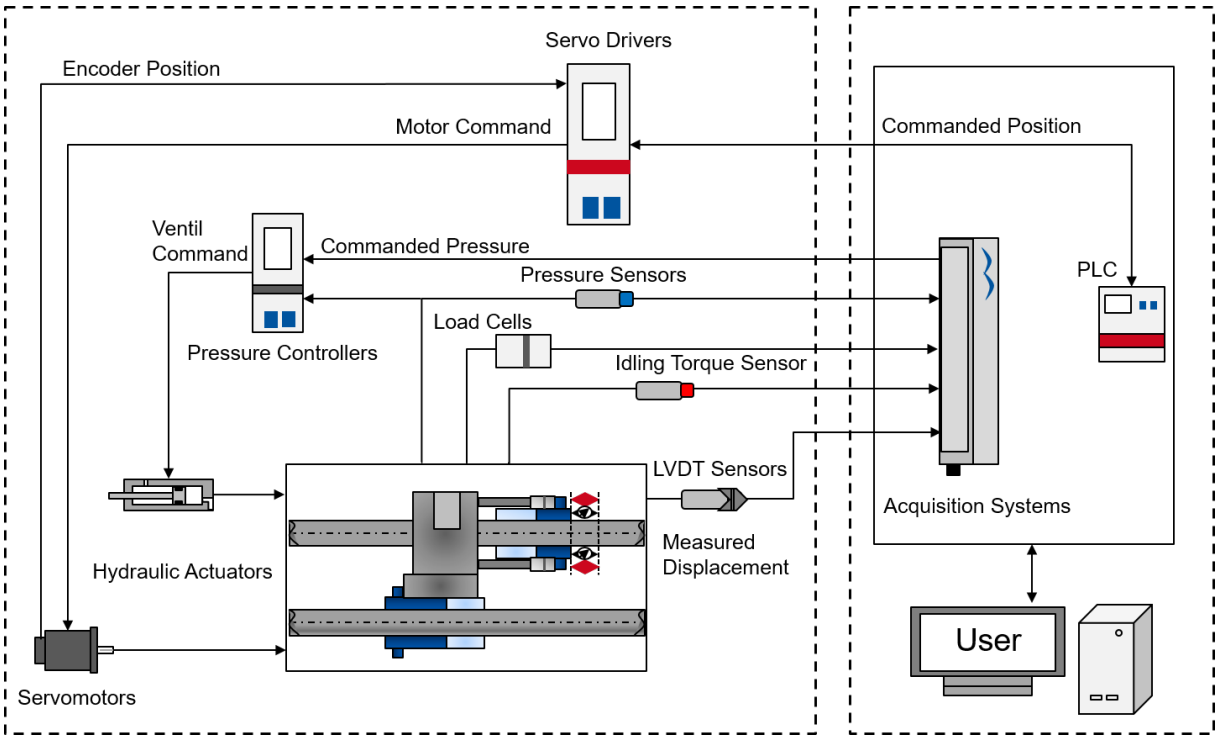

Figure 24: Signals flow between experiment, control and acquisition systems

Source: original.

5.1 Experiment Components

In this section a brief description of the main components that compose the experiment is presented.

5.1.1 Double Nut Ball Screw

In this work two different ball screw systems were used. One was used as a support to carry out the hydraulic system and the load sensors. The second ball screw was used to evaluate the tests, being the one that receives the structural and thermal stresses. Table 1 shows the specifications of the two used ball screws.

Type	Nominal Diameter	Nominal Lead	Ball Diameter	Preload
Evaluate	40 mm	10 mm	6 mm	4.2 kN
Support	40 mm	15 mm	-	-

Table 1: Specifications of used ball screws

5.1.2 Sensors

With the purpose of acquiring data from the experiment and accomplishing the specifications mentioned in this final project work, a set of sensors were used. This section describes characteristics and the role of each sensor used in this work.

5.1.2.1 Pressure Sensor

As can been seen in Section 5.1.4, the pressure controllers use the internal pressure in the hydraulic actuators chambers as a feedback variable to control the force outputted by the hydraulic actuators. Thus, four pressure sensors are used in this experiment. Each par of pressure sensors is allocated at the retract flow and extend flow port from each hydraulic piston, as indicated by the elements 9, 10, 11 and 12 in Figure 29.

Under the circumstances mentioned above, the pressure transmitter from IFM GmbH for industrial applications was used. According to the specifications, the sensor has a reliable detection of system pressure in industrial applications and high shock and vibration resistance, providing a measuring range of 0 to 100 bar.

5.1.2.2 Load Sensor

As explained in Section 3.4.1, the necessary displacements q are determined by solving the linear system 3.16 where F describes the total axial force on the rolling elements. Therefore, to obtain the resulting axial force F, a tension and compression force

sensor from ATP Messtechnik GmbH (2018) for heavy applications was used, as shown in Figure 25. According to the specifications, the force sensor has a great rigidity and a compact design, enabling a wide measurement range (up to 50 kN).

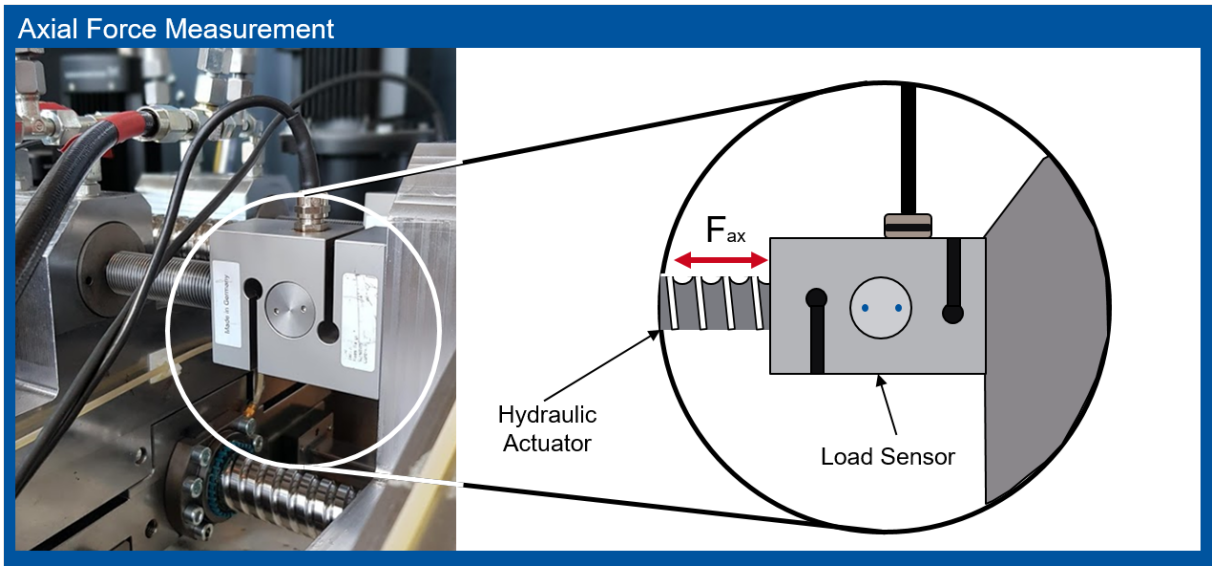

Figure 25: Measuring setup with load sensor

Source: original

5.1.2.3 Friction Torque Sensor

Friction torques without external forces influences are measured by means of a bending beam attached to the nut. At the free end of the bending beam there is a round plastic attachment (shown in red in Figure 26), which hangs between two angle stops fastened on the table and aligned parallel to the screw shaft. A rotation of the ball screw shaft leads to a translational movement of the nut, so that the bending beam presses against one of the angles as a result of the resulting friction torque and slides along it. This results in a deflection of the beam, which is detected by two arranged as a full bridge strain gauges. According to the stored calibration, the resistance change of the strain gauge can be assigned a friction torque. Since in this arrangement only the friction torque to be measured and a negligible friction force between the plastic attachment and the angle are in the force flow, this approach provides comparatively good results. The structure is shown in Figure 26.

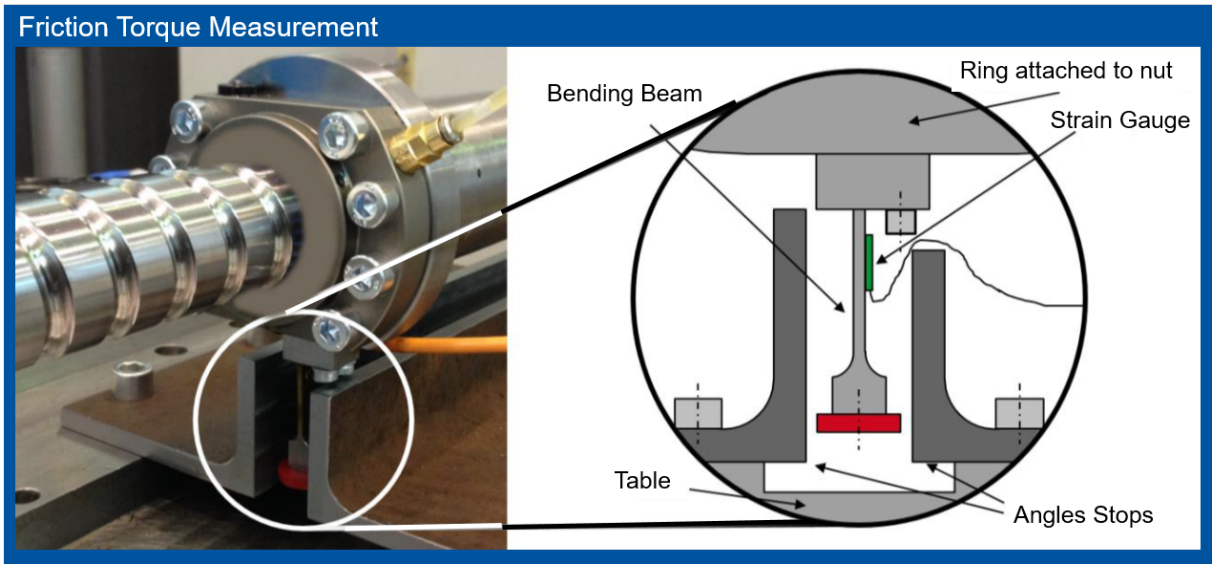

Figure 26: Measuring setup with bending beam

Source: original

5.1.2.4 LVDT Displacement Sensors

To obtain the axial displacements between between bench nut and screw, two displacement sensors were mounted parallel to each other in a distance of 10 mm in a self-made structure. The structure is coupled to a second ball screw that is connected on the same screw shaft from the main ball screw. This sensor arrangement allows to detect tilts between nut and screw shaft. To guarantee a high resolution the sensors are calibrated to measure with a deviation lower than 1μm. The structure is shown in Figure 27.

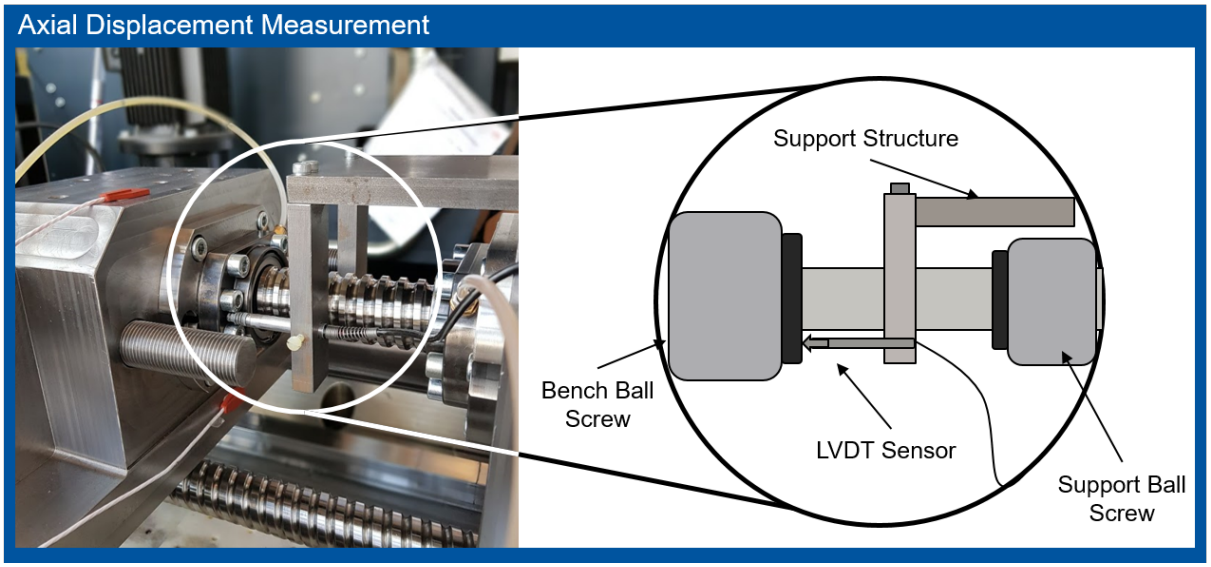

Figure 27: Measuring setup with LVDT Sensors

Source: original

5.1.3 Programmable Logic Controller

According to the Bosch Rexroth IndraLogic L20 System Description (2011), the IndraLogic L20 is a compact small control that includes a standardized I/O system on the basis of terminal technologic and is designed for logic applications. The system engineering software IndraWorks was used in this project to deal with the hardware integration and program the movement logic and the human-machine interface. The software allows the user to create a PLC program project mixing different industrial programmable logic controllers languages. In this project structured list and function blocks languages were used which, combined, helped to reduce the programming time, allowing for a fast hardware integration.

5.1.3.1 Logic and Human Machine Interface

To develop the software, first it was necessary to have a clear understanding of the specifications, according to the following criteria:

1. control the servomotors with accuracy;

2. control the electrical interlocks;

3. support manual movement from the motors;

4. have an intuitive and informative interface.

Before starting software development, it is a critical process to be aware of software development methodologies. These provide high-level programming skills to build a bridge between the engineering problem and the solution. A strategy for modeling a computing problem is through a state machine. In order to design the PLC software to achieve the specifications described above, a state machine was modeled due its efficiently and compact representation.

5.1.3.2 State Machine

State machines are represented using state diagrams. The output of a state machine is a function of the input and the current state. The operation of a state machine begins from a start state, on a successful transition it ends up in an accept state. The transition takes place based on the inputs provided, a current state depends on the past state of the system. A transition is enabled based on certain conditions and indicates a state change, an action describes an activity performed at the given moment.

The state machine modeled can been sen in Figure 28.

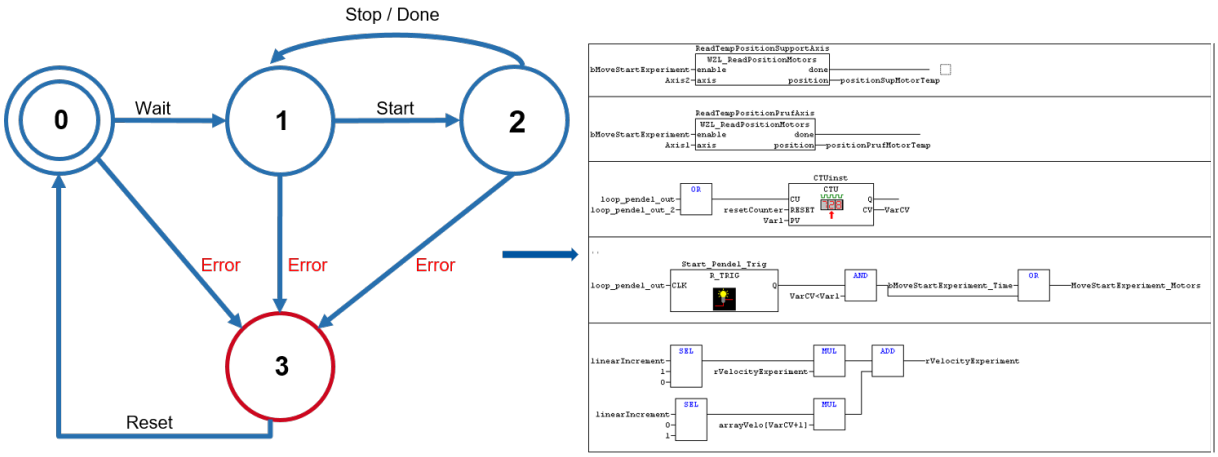

Figure 28: PLC logic state machine

Source: original.

States Description:

0. **Initialize:** initial state, where default configurations and parameters for all system external devices communication, like servomotors and linear encoders, are set;

1. **Waiting user:** the system is ready to start. This state waits until the user presses start;

2. **Experiment Movement:** after the user presses start, the software starts to control the servomotors and to acquire data from the linear encoders;

3. **Error:** if an error occurs, this state stops the servomotors and leads to the initial state when the reset button is pressed.

5.1.4 Hydraulic System

Due to the fact that the experiment must simulate working conditions in ball screw drivers, a hydraulic system is required. It consists of two hydraulic actuators, four pressure reducing valves, two fluid pressure controllers and a hydraulic pump. The main purpose of the hydraulic system is to provide the necessary amount of force output by the hydraulic piston, thus simulating an axial machine process force such as a milling force.

The hydraulic pump (1) provides the full pressure required by the system. The reduction valves (2, 3, 4 and 5) control the amount of flow rate handed out to the hydraulic pistons (6 and 7). Since this is a closed circuit, the outlet fluid must be returned to the tank (8). The valves (2 and 5) are electronic pressure reducing valves, each controlled by a different pressure controller.

The control pressure modules are based on classical control theory, using a proportional, integral and derivative parallel architecture. The control gains were defined empirically. The control modules act by controlling the vent opening of the 2 and 5 electronic pressure reducing valves using the internal pressure in the left chamber of the hydraulic actuator as a feedback variable, allowing more or less flow rate, consequently increasing or decreasing the pressure inside the hydraulic actuator.

The hydraulic circuit from the system can be seen in Figure 29.

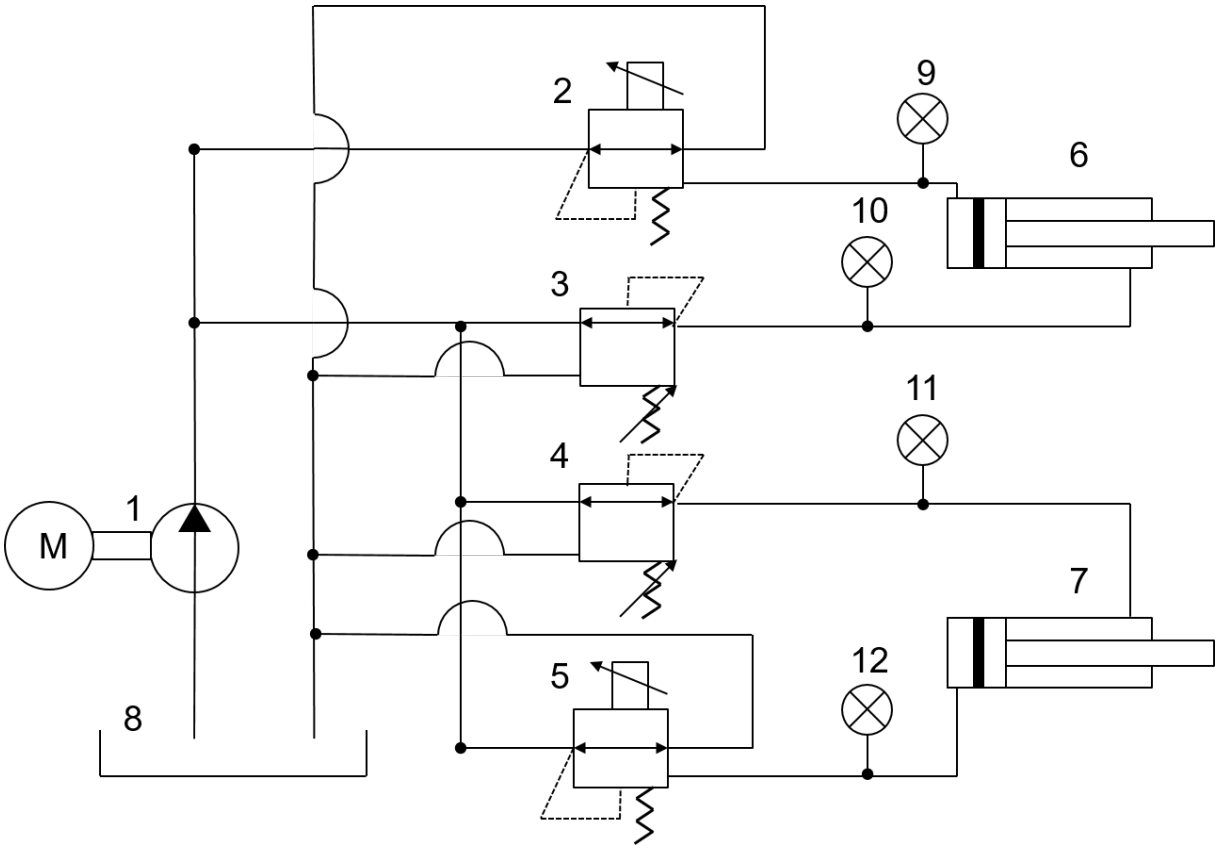

Figure 29: Hydraulic circuit

Source: original.

5.2 Data Synchronization and DAQ Software Development

Regarding the assembly of all sensors, synchronization of acquisition data and integration of all acquisition systems, the National Instruments System Engineering Software LabVIEW was used. Its graphical programming syntax reduces programming time, providing a fast instrumentation integration.

To develop the software, first, it was necessary to have a clear understanding of the specifications, whose topics are listed below:

1. develop a monitor online software in which could be possible to integrate all the data acquisition from the sensors;

2. acquire position data from an external PLC;

3. synchronize the device's reference sample rate (clock);

4. record all the data into a TDMS file;

5. support load profiles through external CSV files;

6. have an intuitive and informative interface.

5.2.1 Synchronization and PLC Data Interconnection

Most of the engineering applications areas require precise control and synchronized data acquisition. Timing and synchronization have an important role in any system's design applications. If the data acquired is not appropriately correlated in time, that is, synchronized, then the analysis and the conclusions from the data are inaccurate, what invalidate any result or engineering application purpose [23].

For this Final Project Work, the National Instruments acquisitions devices run at a different sample rate from the Programmable Logic Controller linear encoders data acquisition and it is possible to synchronize their timing sample acquisition via a reference clock in this case using the local computer to this task.

Due to interconnect the PLC data with the acquisition system the OPC UA (Open Platform Communications Unified Architecture) technology was used. According to [24] OPC is the interoperability standard for the secure and reliable exchange of data in the industrial automation scope and in other industries. It is platform independent and ensures the seamless flow of information among devices from multiple vendors.

5.2.2 External Data Saving

One of the specifications listed on section 5.2 was that the acquisition software must record all the data into a TDMS file, to be able that the producer-consumer multi-process synchronization problem was adapted to this work.

Based on Master/Slave architecture, this multi-process synchronization problem enhances the data sharing between many loops running in parallel and at different sample rates. By Queues functions in LabVIEW, it is possible to acquire the data from one process (producer) and add them in one queue, called as the buffer. Therefore, this large amount of data from the buffer queue might have to be used for showing control parameters by a monitoring interface for the user, or execute some post-calculation, or record the data into a tdms file - consumers. Instead of programming all these tasks in one single loop, which might impair both the system data flux logic and the synchronization,

the Producer/Consumer allows the communication through different loops, one for each task. Thus, the software can execute their processes at an appropriate sample rate and its their own pace, accomplishing the specifications for data acquisition, post processing and synchronization.

6 ANALYSIS OF THE THERMAL-ELASTIC MODEL

To validate the model created in this work, two types of tests were performed on the test bench described in Chapter 5, which are divided into static and dynamic as shown in Figure 30.

The static test is characterized by the measurement of axial stiffness without thermal influences. The dynamic test is performed with relative movement of the ball screws, then friction forces are measured which consequently allows determining the thermal boundary conditions, after, axial stiffness is measured considering thermal influences. Therefore, the measured relative axial displacement of nut and screw shaft under external load and thermal influences is compared to calculated results.

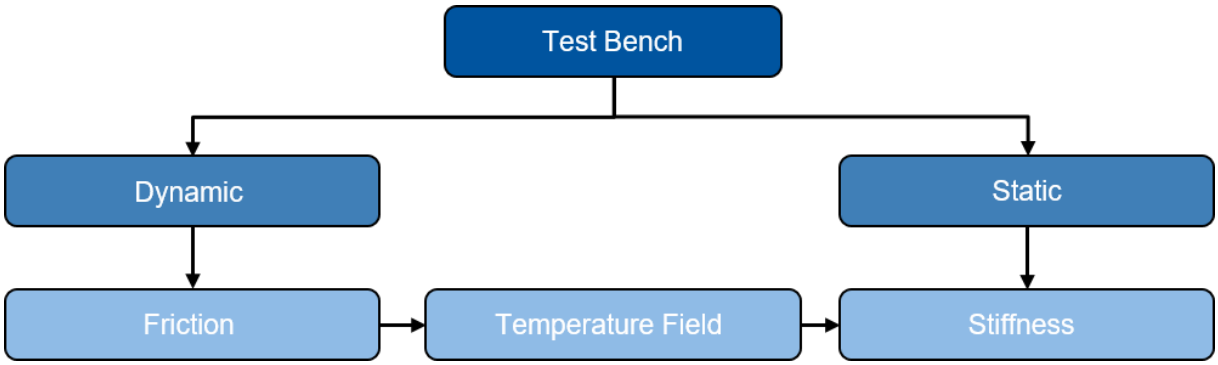

Figure 30: Carried out test series

Source: original.

Figure 31 shows the MTPlus model used to simulate the tests described above. The model represents a double nut screw that receives variations of external axial forces in the first nut, a mechanical support is placed at the end of the screw shaft representing that at this point the system is fixed.

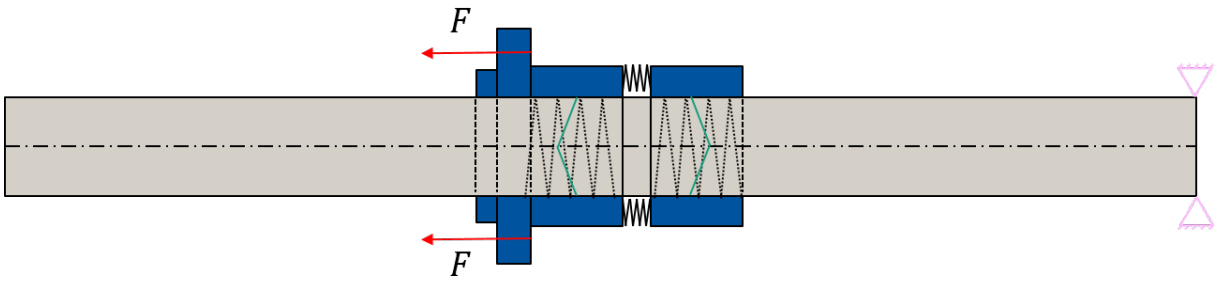

Figure 31: Ball screw model created in MTPlus

Source: original.

6.1 Analysis of Structural Static Behavior

The load displacement curve of the bench ball screw was measured in the range of approximately 0 to -3 kN in a controlled environment of 24 °C indicating that there is no temperature gradients between the nuts and the screw shaft. For the same range and thermal environment, the behavior of the ball screw was simulated using the MT-Plus in steps of 0.5 kN. Figure 32 shows a comparison of measured and calculated load displacement curves.

The curves show a nearly linear slope for tensile forces. As can be seen in Figure 32, the calculated load displacement curve coincide with the measured one. From the curves, 8 stiffness values were calculated representing the tensile stiffness from the measured and calculated values. Table 2 shows the values that were calculated for tensile forces between -2500 kN until -1000 kN.

The measured values are the mean of three measurements for each step of 0 until -3kN, with standard deviation given. The mean deviation between measurements and calculation for single values is lower than 21%. A few possible causes for the deviations are manufacturing tolerances, like the pitch error, or an inaccurate preload, another cause is that MTPlus calculate the initial equilibrium state where there are no node displacements and only the initial forces act on the system, which e.g. the preload force. The calculation leads to an initial displacement which can not be measured and causes an initial deviation between the measured value which starts in 0 μm and the calculated in approximately 0.3 μm.

Measurement			Calculated			Deviation
N	μm	N/μm	N	μm	N/μm	%
-2500	-1.330	1878.71	-2500	-1.677	1490.76	-20.649
-2000	-1.076	1857.36	-2000	-1.322	1512.86	-18.547
-1500	-0.824	1820.39	-1500	-0.991	1513.78	-18.843
-1000	-0.568	1758.71	-1000	-0.644	1552.0.7	-11.745

Table 2: Stiffness static test values of analyzed ball screw

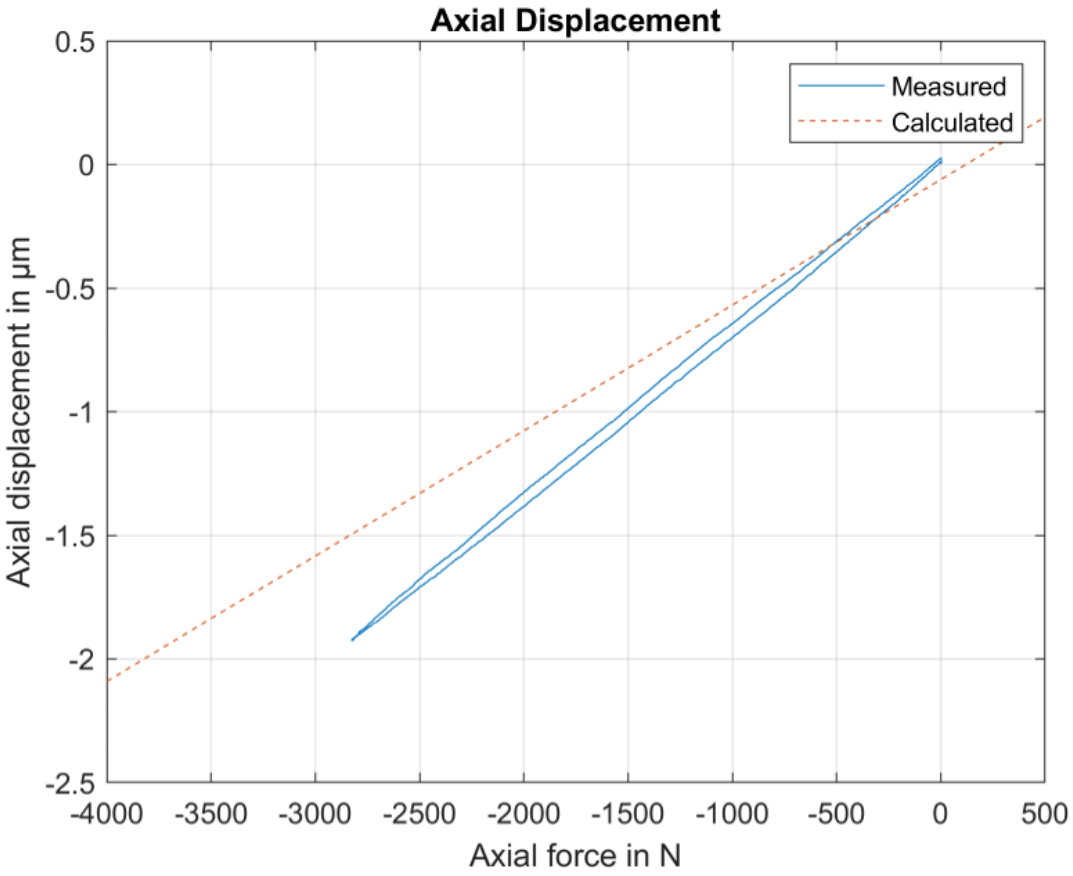

Figure 32: Load displacement curves of static analyses

Source: original.

For each calculation step of 0.5 kN, there are detailed results for the rolling element contact characteristics. In the following, there are discussed for a tensile load of -2.5 kN.

Figure 33a shows the matching nodes displacements. In the figure, each point marks a node on the beam, containing a refined elements mesh in the rolling contact zone. The deformation is linear until the start of the rolling contact zone. From that point,

the relative displacement between nut and screw shaft decreases. The total displacement of the first nut is higher, than the second nut. This is due to the load position which is directed applied to the first nut. Therefore, the load distribution shown in Figure 33b depends on the load position.

The axial component of the contact force in the first nut is in the range of 50 to 60 N and the second nut, it ranges from -30 to -20 N, this is due the fact that the preload force act on opposite direction in each nut. As a result of the elastic deformation of the screw shaft and nuts, the rolling element contact characteristics differ in each nut.

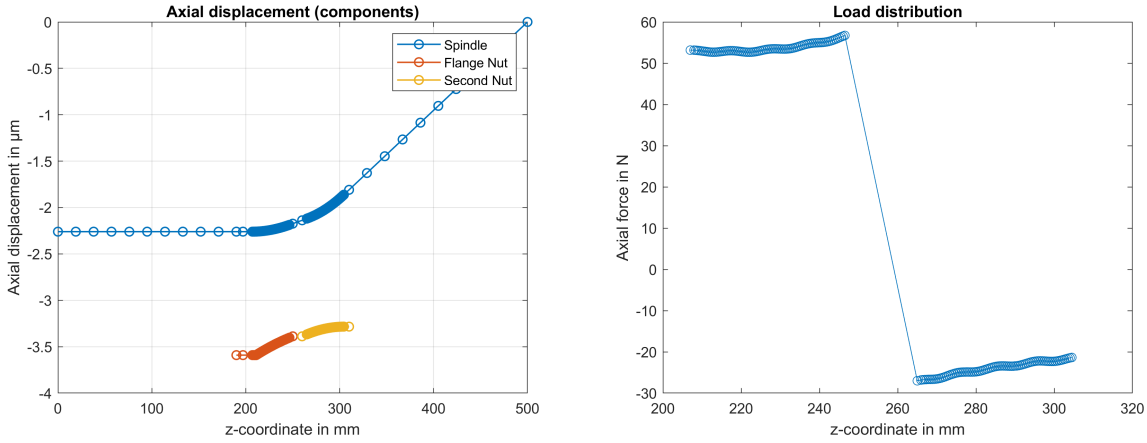

(a) Nodes displacement (b) Load distribution in the rolling elements

Figure 33: Load and displacement results for -2.5 kN tensile load

Source: original.

6.2 Analysis of Structural Dynamic Behavior

For the structural dynamic behavior, a friction torque curve without external forces and moments was measured in the range of 5 until 1000 rpm (Figure 34). As can been seen in the Section 3.2.4 the total heat generated Q_{ns} is the product between the friction moment and the angular speed. Thereby, for the same range each Q_{ns} was calculated and used as a thermal boundary condition in the MTPlus thermal model.

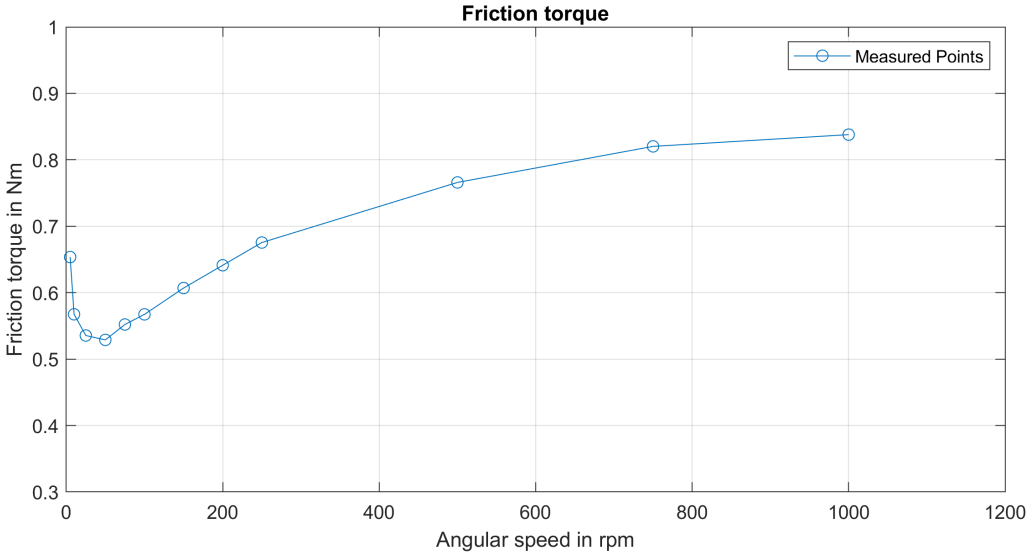

Figure 34: Friction torque curve

Source: original.

The replication of these simulations in the real experiment can last a long period of time, due the fact that the nut needs to travel long distances to reach the temperature simulated, additionally causing wear, reducing the useful life of the component. Thereby, an artifice was used. A heating mat coupled to a temperature controller was placed on the table linked to the bench ball screw, also Pt100 sensors were placed on the top and on the bottom of the table, on the nut and on the screw shaft. It can been seen in Figure 35.

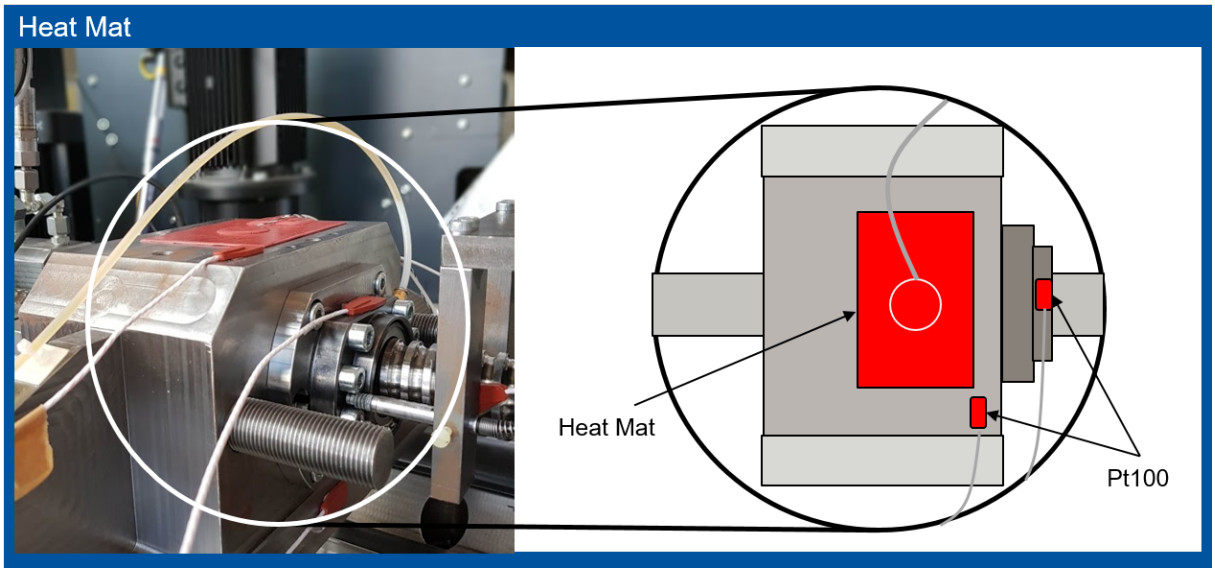

Figure 35: Heat mat artifice and temperature sensors

Source: original.

For each simulated heat input, there are detailed simulation results for the thermal system behavior and the contact characteristics of the rolling elements. In the following for a angular speed of 150 rpm was the experimented validated, since this interval represents a real working velocity and it represents a working gradient temperature between the first nut and the screw shaft of approximately 1 °C which is not harmful to the system.

The calculated temperature field is shown in Figure 36, it shows the calculated temperature for each position in the ball screw model. The warmer component is the first nut due its contact surface with the table where the heat mat is placed. The second nut and the screw shaft follow the same temperature profile. Near to position 200 mm the first nut shows a small temperature decline, this is caused by the component geometrical form.

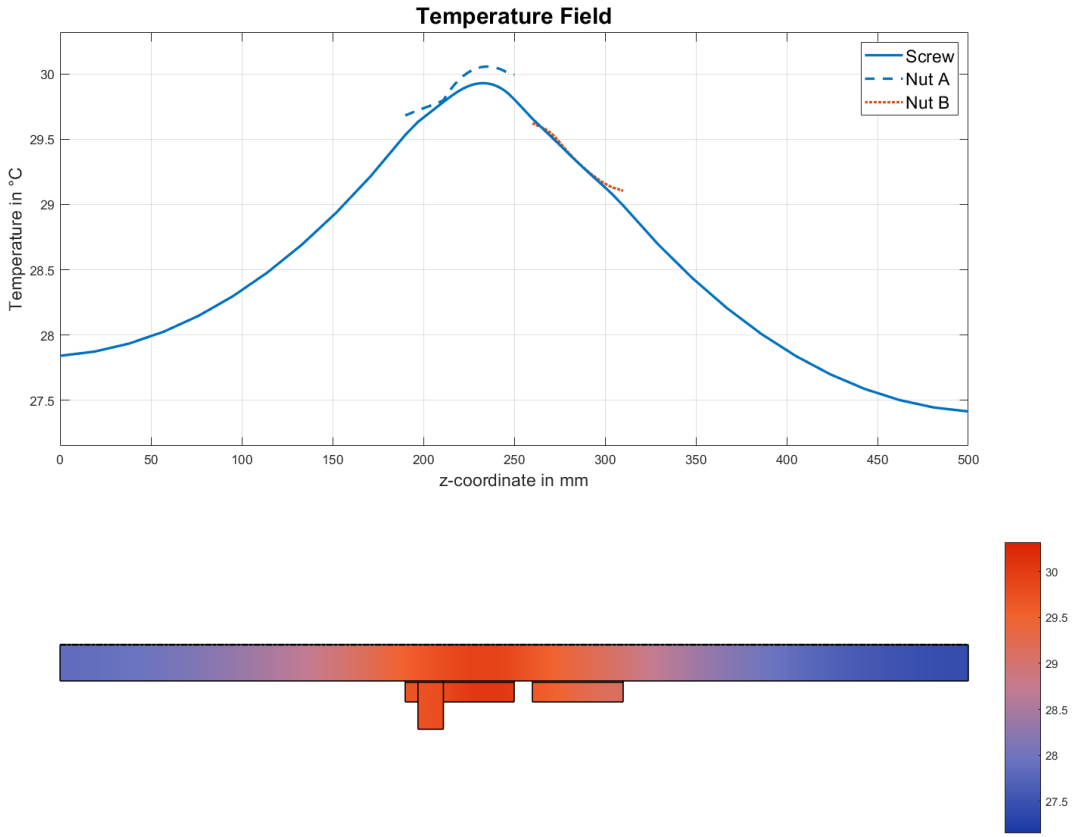

Figure 36: Temperature field results using the heat mat

Source: original.

The load displacement curve was measured in the range of approximately 0 until -3 kN. For the same range, the behavior of the thermal ball screw was simulated using the MTPlus in steps of 0.5 kN. Figure 37 shows a comparison of measured and calculated load displacement curves. As in the static test the curves show a nearly linear slope for tensile forces. As can be seen in Figure 37, the calculated load displacement curve nears the measured curve. From the curves, 8 stiffness values were calculated, representing the tensile stiffness of the measured values and calculated values.

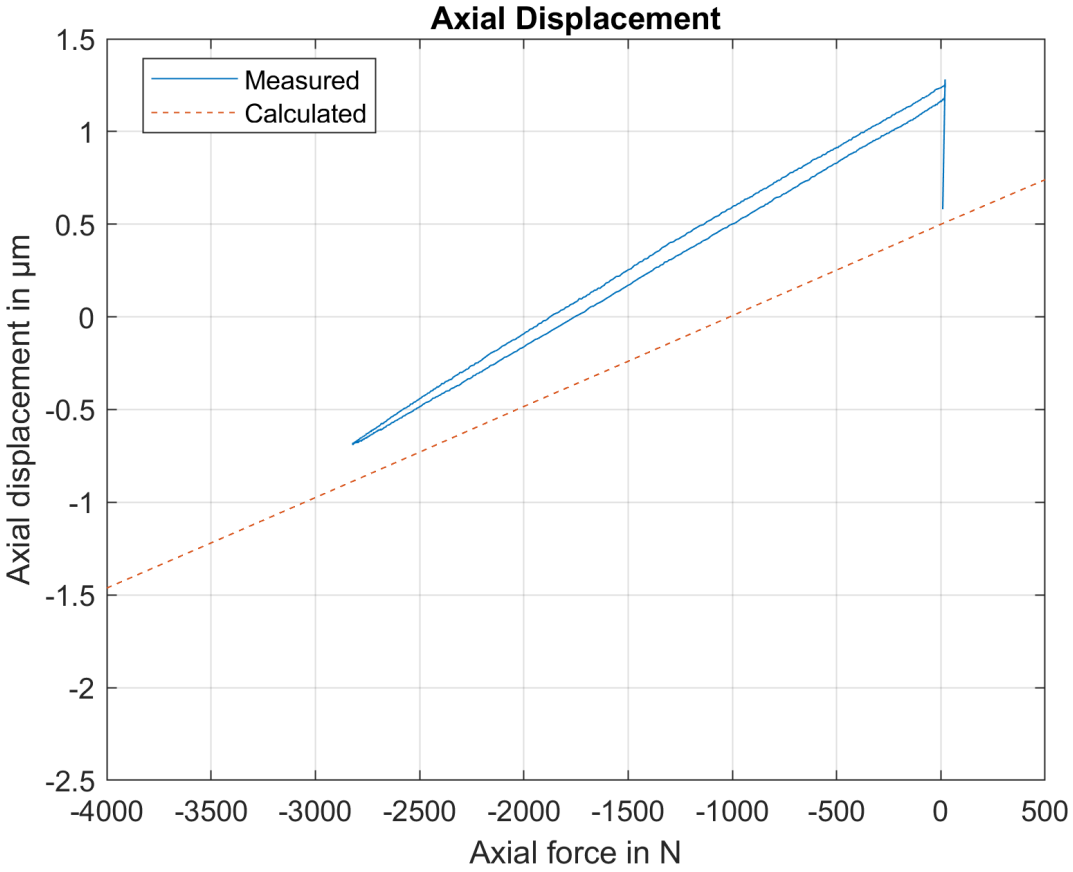

Figure 37: Load displacement curves of thermal analyses

Source: original.

Table 3 shows the values that were calculated for the tensile forces between -2500 kN to -1000 kN.

Measurement			Calculated			Deviation
N	μm	N/μm	N	μm	N/μm	%
-2500	-0.4403	5677.94	-2500	-0.2921	8557.08	-50.70
-2000	-0.0923	21666.12	-2000	-0.0291	68692.57	-217.05
-1500	0.2547	-5889.28	-1500	0.2332	-6431.90	-9.21
-1000	0.5263	-1900.05	-1000	0.4996	-2001.55	-5.34

Table 3: Stiffness dynamic test values of analyzed ball screw

The measured values are the mean of three measurements for each step of 0 until -3 kN, with standard deviation given. Unlike the static test, the test with thermal influences showed greater deviations from the measured values for those calculated. Some of

the possible causes for the larger deviations would be an inaccurate approximation of the temperature gradients between the model components, due to the fact that not all the support structures that are in the experiment were taken into account in the model created, such structures are also affected to thermal variations and consequently by thermal forces.

6.3 Analysis of Static and Dynamic Behavior

The results for static and dynamic behavior showed significant differences as can been seen in Figure 38. A compression displacement between the static and dynamic load displacement curves was observed, both for the calculated and measured values.

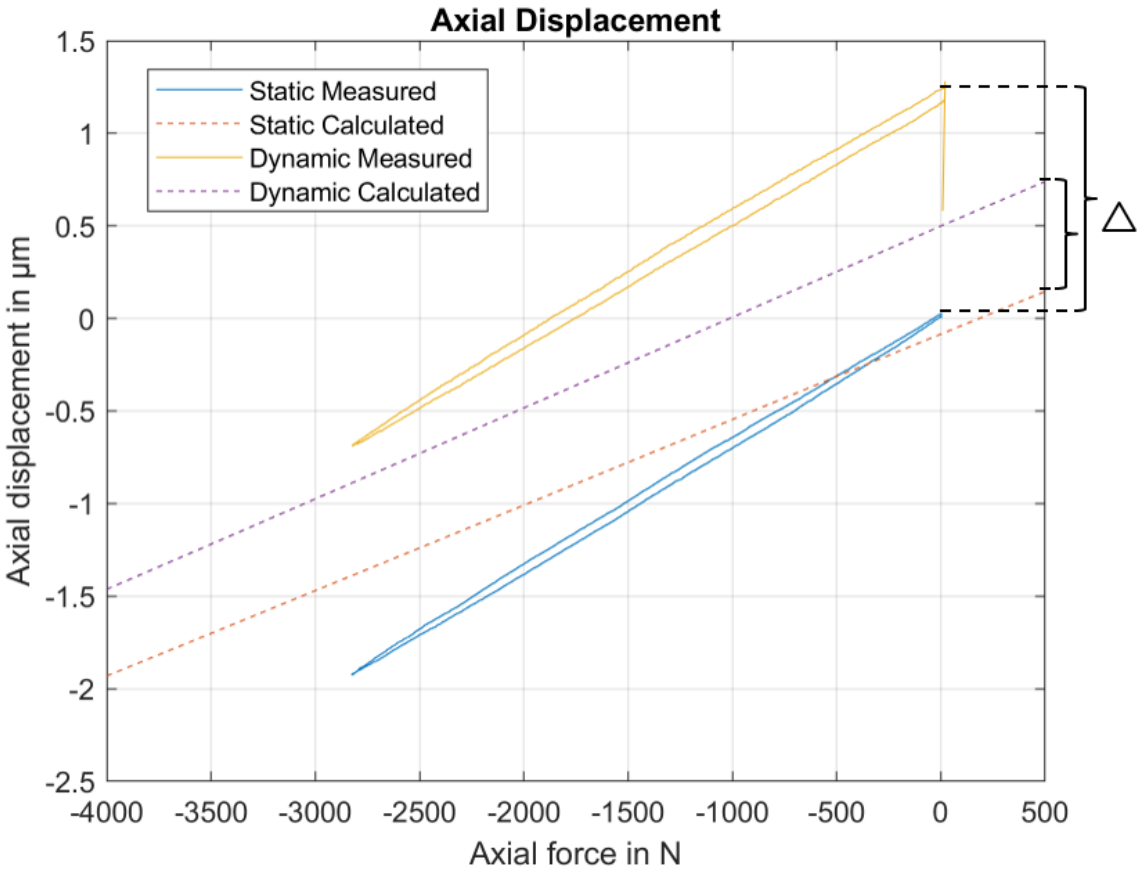

Figure 38: Load displacement curves of static and dynamic analyses

Source: original.

The compression displacement was caused by the positive temperature gradient between the first nut and the second one. Thereby, leading to a gradient in the normal

forces between the two nuts of the double nut ball screw model. In the static model evaluated without thermal influences, the normal loads between each nut and screw shaft were approximately equal, as can been seen Figure 39a. On other hand, Figure 39b shows the model evaluated and calculated with thermal influences, it showed higher normal forces acting in the second nut as on the first nut, resulting in a compressive force. The gradient is caused due that one of the nuts is warmer than the another, resulting in an geometry expansion and leading to contact lost between the balls and the raceway grooves.

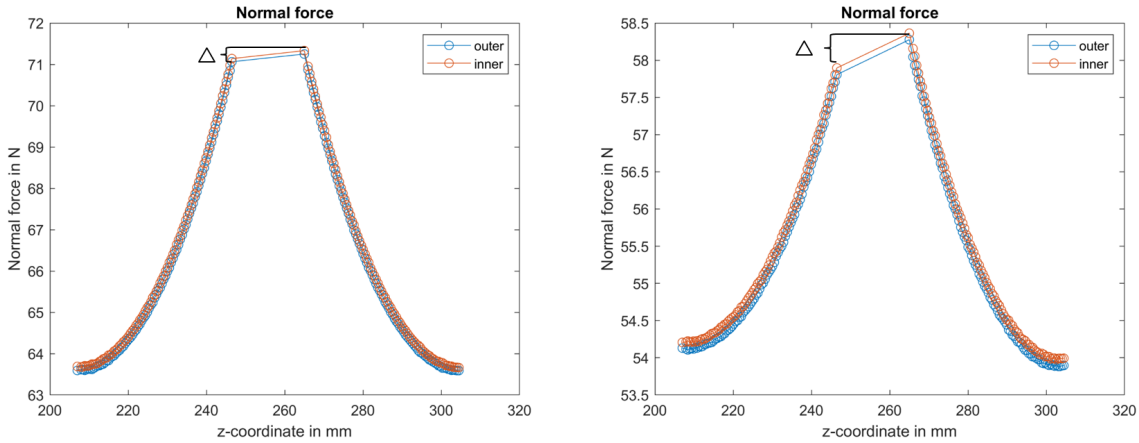

(a) Normal forces for static simulation (b) Normal forces for dynamic simulation

Figure 39: Normal forces comparison for static and dynamic test

Source: original.

A second simulation was performed aiming a negative gradient between the first nut and the second one, the simulated temperature field can been seen Figure 40. In the figure, the second nut is the warmer component and the first nut is following the same temperature profile from the screw shaft. It implicates in a opposite gradient showed in Figure 36. Figure 41b shows the normal forces calculated for the negative gradient. In the figure, the normal forces acting on the first nut were higher than the second nut and a tensile displacement between the first nut and the screw shaft were also calculated. Thereby, axial displacement is dependent to the temperature gradient between nuts and screw shaft.

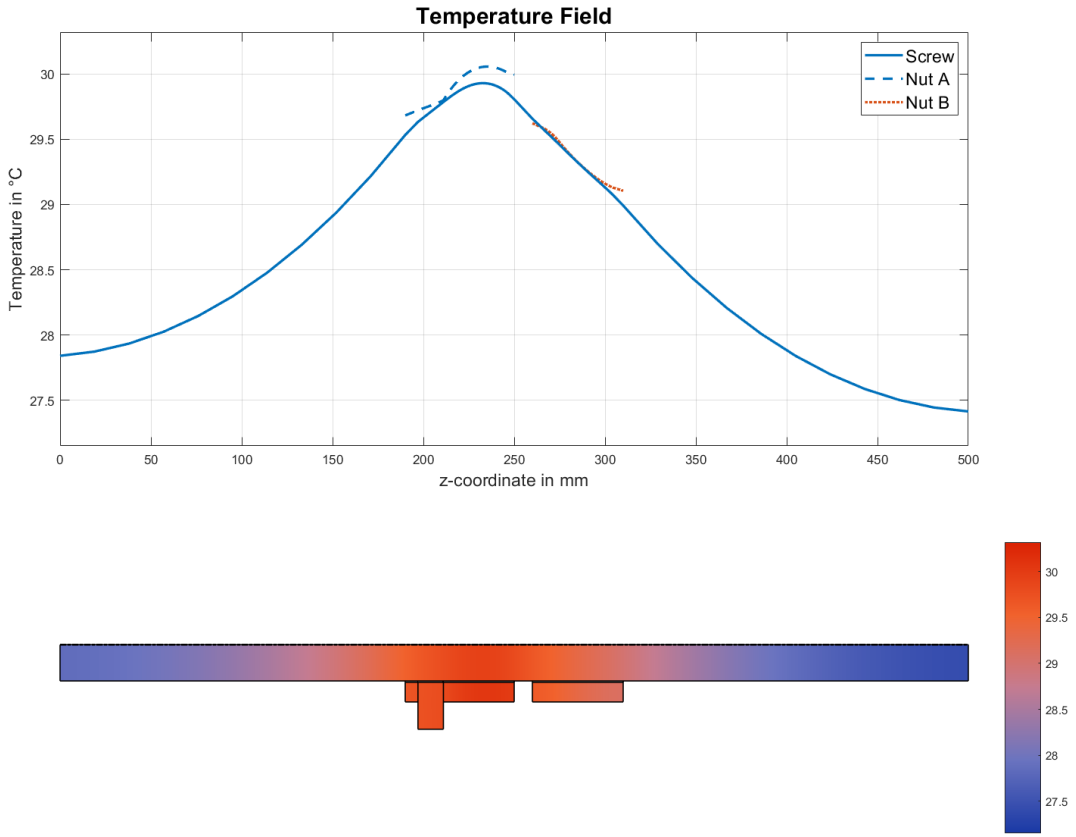

Figure 40: Temperature field for negative gradient between first nut and second one

Source: original.

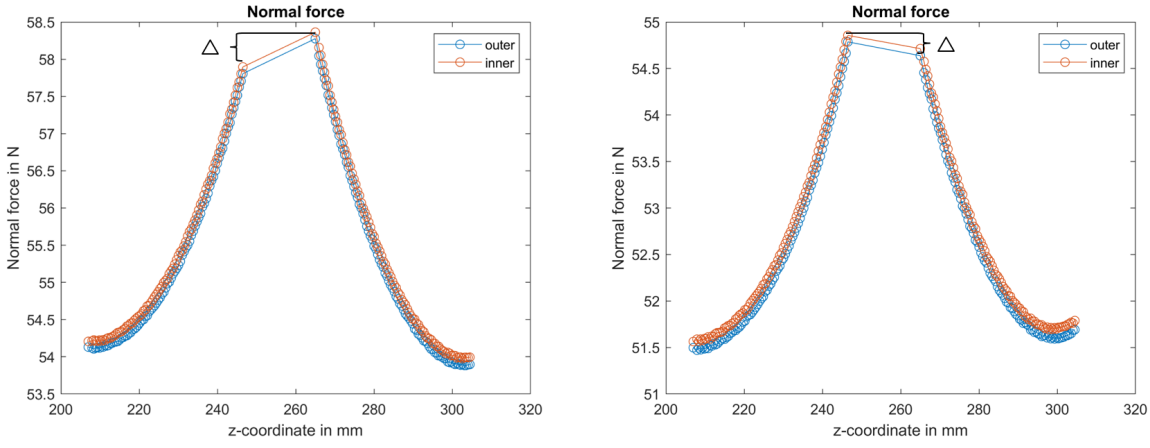

(a) Normal forces first nut warmer than second nut

(b) Normal forces second nut warmer than first nut

Figure 41: Normal forces comparison for different temperature fields

Source: original.

7 CONCLUSION AND OUTLOOK

In the first part of this work a thermal-structural model for ball screws was developed in finite elements. The model was inserted into the software MTPlus for structural simulations created at the WZL. Subsequently, an amplification in the software was performed to map the results of external temperature simulations in 3D models to be used in the structural simulations and accurate results to be achieved.

In the second part an experiment was set up to perform the validations of the models created. In this stage two human interface machines were developed: the first one to control and supervise the components connected to the programmable logic computer, and another one to acquire data from the sensors instrumented in the experiment.

Due to its complex structure, the structural and thermal mechanical behavior of a ball screw still eludes comprehensive simulation understanding. This final project work represents a small piece of the mosaic on this path. It describes the empirical-analytically investigation of the thermal-elastic behavior of ball screws.

The load displacement curves calculated with the linked thermal elastic simulation model show a conformity with the measured curves from the preload double nut screw used in this final project work. After reciprocal working tests, the maximum mean deviation between the measured and calculated values were less than 21% at the -2.5 kN tensile force. It has also been noticed that the stiffness is highly dependent on the temperature gradient between the nuts and the screw shaft.

The MTPLus software, which was expanded in this work, presented significantly accurate results, but it still presents a disparity in relation to the professional simulation software. While the proprietary software allows greater freedom of modeling, the MTPLus fails in this aspect, making the modeling of extra structures limited.

As in this work only a rotationally symmetrical temperature field is assumed, it would be useful to carry out further investigations on a complete, three-dimensional model, in which case the effects of radial displacements can be taken into account. Along with this, the structural-mechanical simulation needs to be transformed from a beam model into a three-dimensional model. In order to further improve the results of the presented calculation method, more precise analytic models should be deposited for the simplified assumed components and structures.

Since the temperature field influences the performing behavior of the ball screw system, an extension in the MTPlus, in which equations from thermal and structural mechanics simulation are solved together, would allow MTPlus to become more dynamically accurate. As a continuation of this approach, a transient calculation could be performed. This could then serve for anticipating the heating on a ball screw. Another application is to use the process-parallel calculation to incorporate current structural stiffness compensation into the machine control. Knowledge of the condition of the overall machine could be used to increase manufacturing quality.

REFERENCES

[1] STEINERT, A. Analyse und simulative Abbildung des thermo-elastischen Verhaltens von Kugelgewindetrieben. Tese (Bachelor's Thesis) — Rheinisch-Westfälische Technische Hochschule Aachen, Aachen, North Rhine-Westphalia Germany, 27/03/2017.

[2] OYANGUREN, A.; LARRAÑAGA, J.; ULACIA, I. Thermo-mechanical modelling of ball screw preload force variation in different working conditions. The International Journal of Advanced Manufacturing Technology, Springer Nature, v. 97, n. 1-4, p. 723–739, apr 2018.

[3] ALTINTAS, Y. et al. Machine tool feed drives. CIRP Annals, Elsevier BV, v. 60, n. 2, p. 779–796, 2011.

[4] BRECHER, C. et al. Modelling of ball screw drives rolling element contact characteristics. CIRP Annals, Elsevier BV, v. 67, n. 1, p. 409–412, 2018.

[5] LTD, N. Chapter 2 Construction of Ball Screws and Their Functional. [S.l.].

[6] FENG, G.-H.; PAN, Y.-L. Investigation of ball screw preload variation based on dynamic modeling of a preload adjustable feed-drive system and spectrum analysis of ballnuts sensed vibration signals. International Journal of Machine Tools and Manufacture, Elsevier BV, v. 52, n. 1, p. 85–96, Jan 2012.

[7] VERL, A.; FREY, S.; HEINZE, T. Double nut ball screw with improved operating characteristics. CIRP Annals, v. 63, n. 1, p. 361–364, 2014.

[8] OLARU, D. et al. A new model to estimate friction torque in a ball screw system. Product Engineering: Eco-Design, Technologies and Green Energy, p. 333–346, 01 2005.

[9] KRÖMER, M. Simulation thermischer Einflüsse auf das Betriebsverhalten von Spindel-Lager-Sys-temen. Tese (Bachelor's Thesis) — Rheinisch-Westfälische Technische Hochschule Aachen, Aachen, North Rhine-Westphalia Germany, 16/07/2018.

[10] GANJI, D. D.; SABZEHMEIDANI, Y.; SEDIGHIAMIRI, A. Conduction–convection heat transfer. In: Nonlinear Systems in Heat Transfer. [S.l.]: Elsevier, 2018. p. 35–104.

[11] SUKHATME, S. P. A textbook of heat transfer. 4th edn.. ed. Hyderabad: Universities Press, 2013. ISBN 8173715440.

[12] MILLS, A. F. Heat transfer. International student ed. Homewood, Ill.: Irwin, 1992. ISBN 0256128170.

[13] MO, J. P.; CHEUNG, S. C.; DAS, R. Steady-state heat conduction systems. In: Demystifying Numerical Models. [S.l.]: Elsevier, 2019. p. 61–85. ISBN 9780081009758.

[14] INCROPERA, F. P. et al. Foundations to heat transfer. 6. ed., internat. student version. ed. Singapore: Wiley, 2013. ISBN 0470501960.

[15] MORGAN, V. T. The overall convective heat transfer from smooth circular cylinders. In: Advances in Heat Transfer Volume 11. [S.l.]: Elsevier, 1975, (Advances in Heat Transfer, v. 11). p. 199–264. ISBN 9780120200115.

[16] REDDY, J. N. An introduction to the finite element method. 3rd ed.. ed. New York NY: McGraw-Hill Higher Education, 2006. (McGraw-Hill series in mechanical engineering). ISBN 978-0072466850.

[17] WILLIAMSON, F. An historical note on the finite element method. International Journal for Numerical Methods in Engineering, v. 15, n. 6, p. 930–934, 1980. ISSN 0029-5981.

[18] COOK, R. D. Concepts and applications of finite element analysis. 4th ed.. ed. New York, NY: Wiley, 2001. ISBN 0-471-35605-0.

[19] RUSSELL, R. C. Computer Finite Element Simulation In Mechanical Design. Tese (Master's Thesis) — Vanderbilt University, Nashville, Tenesse United States Of America, 11/2013.

[20] WECK, M. et al. Stabilitätsanalyse bei der hsc-bearbeitung. WT Werkstattstechnik online, v. 93, p. 63–68, 2003.

[21] TÜLLMANN, U. Das Verhalten axial verspannter, schnelldrehender Schrägkugellager. Tese (Phd's Thesis) — RWTH, Aachen, 1993.

[22] MESYS AG. Ball screws. Available at: <https://www.mesys.ag/>.

[23] National Instruments. Synchronization Explained. Available at: <http://www.ni.com/white-paper/11369/en/>. Accessed in: 14/04/2019.

[24] OPC Foundation. What is OPC? Available at: <https://opcfoundation.org/about/what-is-opc/>. Accessed in: 10/04/2019.

A EXPERIMENT GRAPHICS USER INTERFACE

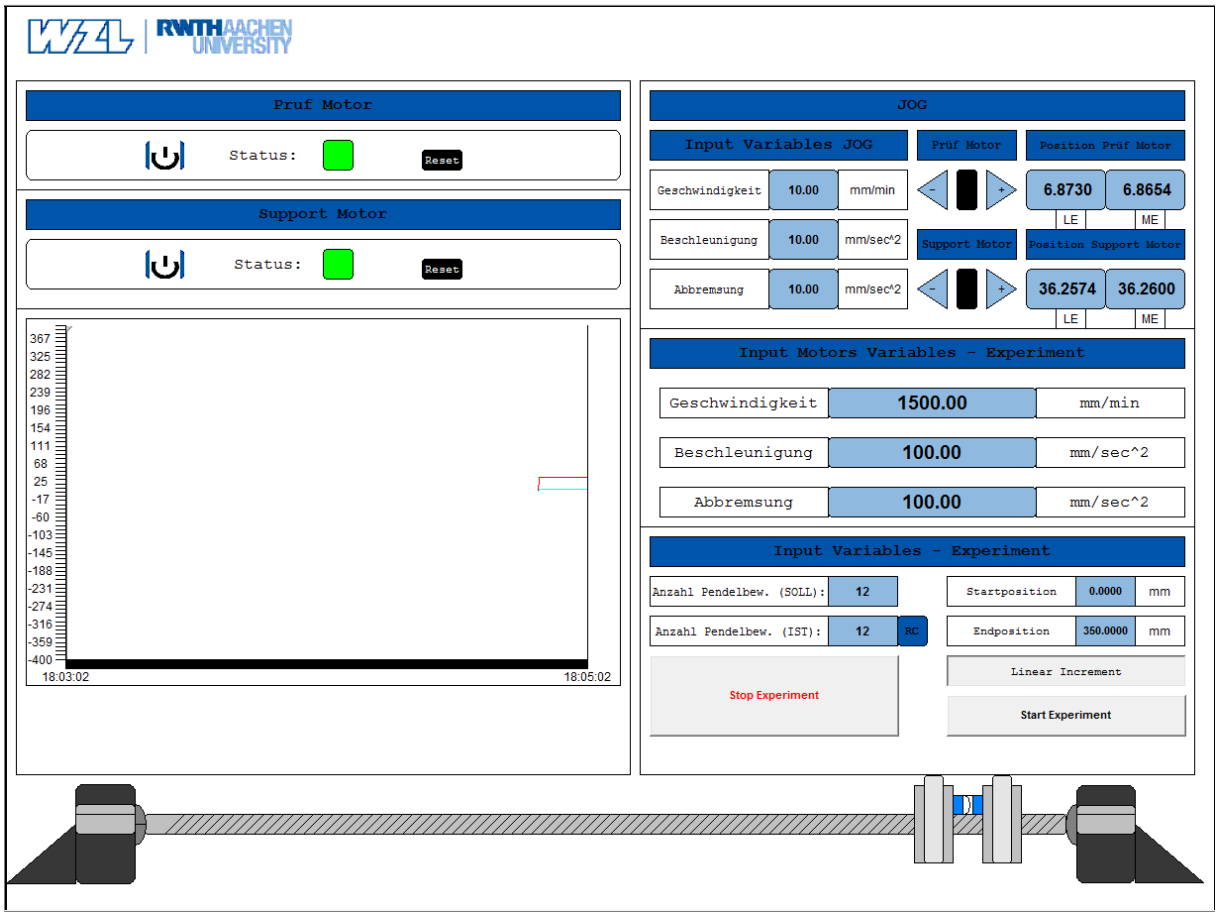

Figure 42: PLC user machine interface

Source: original.

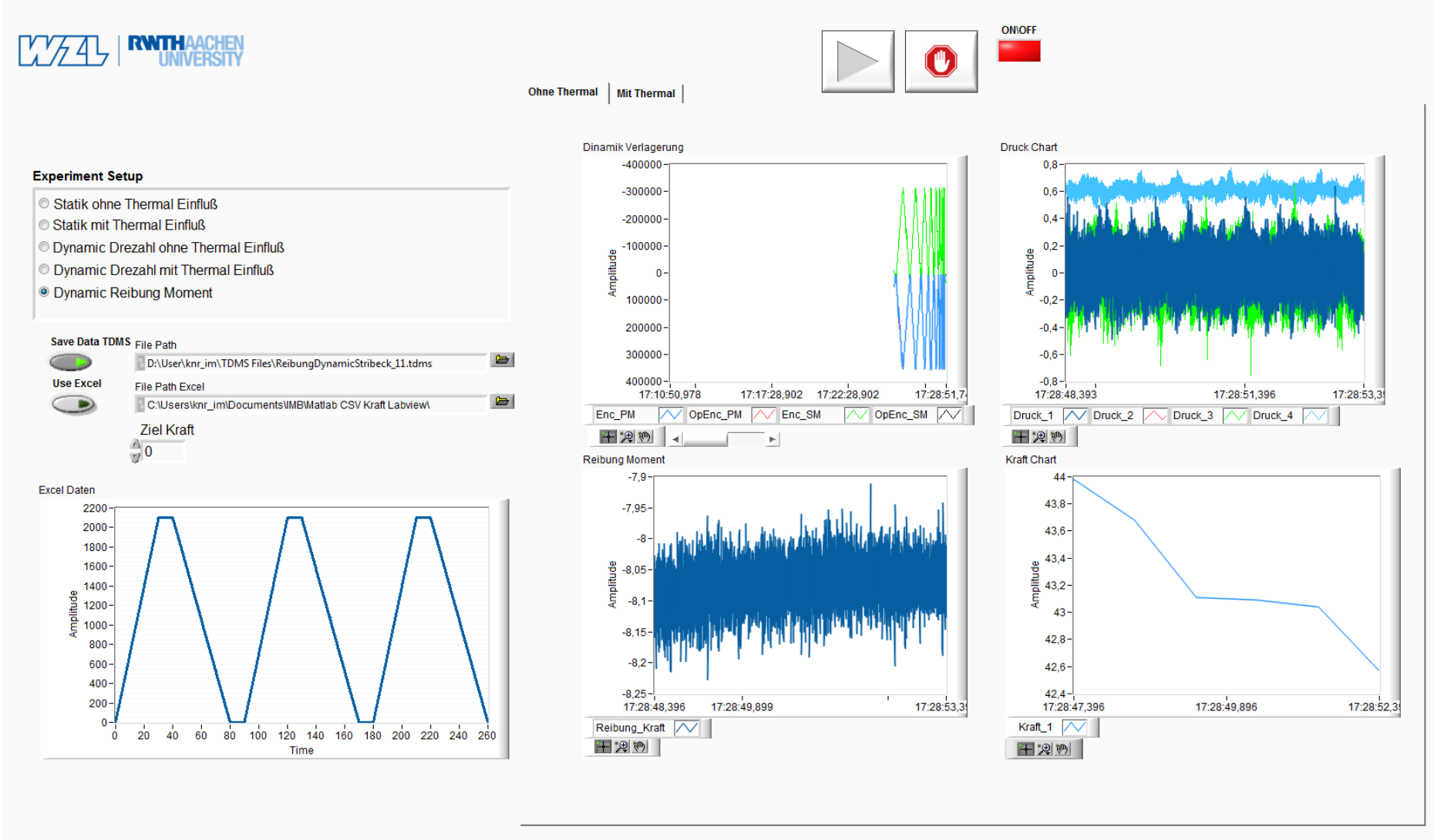

Figure 43: Data acquisition graphic user interface

Source: original.